Ph.D. Dissertation of Natural Sciences

The Development of Scene-based Place Code in the Hippocampal Subregions CA1 and CA3

해마 하위 영역 CA1과 CA3의 장면 자극에 기반한 장소 표상 형성 연구

February 2021

Graduate School of Natural Sciences
Seoul National University
Brain and Cognitive Sciences Major

Hyun-Woo Lee

The Development of Scene-based Place Code in the Hippocampal Subregions CA1 and CA3

Inah Lee

Submitting a Ph.D. Dissertation of Natural Sciences

December 2020

Graduate School of Natural Sciences
Seoul National University
Brain and Cognitive Sciences Major

Hyun-Woo Lee

Confirming the Ph.D. Dissertation written by Hyun-Woo Lee

December 2020

Chair	이 석 호	(Seal)
Vice Chair	이 인 아	(Seal)
Examiner	정 민 환	(Seal)
Examiner	Sébastien Royer	(Seal)
Examiner	이 도 윤	(Seal)

Abstract

When we recall the past experiences, we usually think of a scene which is a combination of what we saw, the sounds we hear, and the feeling we felt at that moment. Since the scene is an essential component of episodic memory, studying how scene stimuli are represented and stored in the brain is important in understanding the processes of formation, storage, and retrieval of our memories. One of the brain regions important for episodic memory is the hippocampus. It has been reported that patients or animals with damage to the hippocampus have trouble with retrieving past experiences or forming new memories. The hippocampus is involved not only in episodic memory but also in the formation of a cognitive map. In particular, the place cells observed in the rodent hippocampus play a key role in these functions. However, research on place cells has mainly focused on the firing patterns of cells during foraging in a space, and it has not been clear how hippocampal cells represent and make use of visual scenes for behavior.

To find how scene stimuli are represented in place cells, I measured spiking activities of single neurons in the CA1, one of the subregions of hippocampus, and the subiculum, a major output of the hippocampus. Neuronal spiking activity was monitored when the rat performed a task of selecting right or left associated to the scene

stimulus presented on monitors. As a result, I found that the place cells in the CA1 and subiculum showed rate modulation according to the scene stimulus. In addition, I also conducted an experiment using a virtual reality system to investigate the neural mechanisms of the formation of a place field based on visual scenes. In this experiment, the rat ran on a virtual linear track as visual cues were added one by one to make a scene-like environment. Neuronal activities of place cells were recorded in the CA1 and CA3 simultaneously to study the neural mechanisms of the development of a place field on the basis of external visual stimuli. Place fields appeared in the CA1 even with a single visual cue, whereas in the CA3, place fields only emerged when a sufficient number of visual cues were collectively arranged in a scene-like fashion. The results suggest that that scene is one of the key stimulus that effectively recruits the hippocampus.

Keywords: hippocampus, CA1, CA3, subiculum, place cell, visual scene

Student Number: 2013-23793

Table of Contents

List of Figures

Background

1. Scene processing in the hippocampus

Hippocampus is known to play an important role in episodic memory (Scoville and Milner, 1957; Zola-Morgan et al., 1986; Eichenbaum, 2000; Squire and Wixted, 2011) and spatial navigation (O'Keefe and Dostrovsky, 1971; O'Keefe and Nadel, 1978; Moser et al., 2008). Recently, scene construction theory (SCT) has been suggested, which explains the involvement of the hippocampus in these two different functions (Hassabis and Maguire, 2007; Maguire and Mullally, 2013). Scenes are an efficient way packaging various information and act as an essential element in process of recall the past, imagining the future, and making plans to go somewhere (Maguire and Mullally, 2013). Therefore, SCT argues that the fundamental function of the hippocampus is scene construction, and episodic memory and spatial navigation involve the hippocampus because they require the scene processing (Hassabis and Maguire, 2007).

The empirical evidence of scene construction theory have been found in human studies. Patients with hippocampal damage had difficulty recalling past episodic memories, and they also showed impairment in the task imagining future (Race et al., 2011), and there were several reports from the patients which they had trouble with imagining a scene (Hassabis et al., 2007b; Andelman et al., 2010; Mullally et al., 2012). In addition, an fMRI study with healthy human subjects reported hippocampal activation during imagining a fictitious scene (Addis et al., 2007; Hassabis et al., 2007a).

The involvement of hippocampus in scene processing has also

been reported in rodent studies. It is known that the hippocampus is not involved in tasks associated with simple cues such as auditory fear conditioning, whereas the hippocampus is involved in contextual fear conditioning (Kim and Fanselow, 1992). Our laboratory also considered scene information processing as the main function of the hippocampus so we conducted a series of experiments to confirm this hypothesis. Previously, it was common to define a scene as several distal cues around the wall of the maze (Hetherington and Shapiro, 1997; Lee et al., 2004; Lee and Kim, 2010). However, it is difficult to know which of the various cues the rat is looking at, and therefore, it is difficult to clarify which part of the scene affects the hippocampal cell activity. So in our laboratory, we used a memory task which allows the experimenter to control what the rat is looking during the task (Kim et al., 2012a). In this memory task, three monitors are installed on the top side of T-maze, and the rat is required to see the visual scene stimulus presented on the monitors to select the side (i.e., right or left) associated with the scene for a reward. We have reported that the inactivation of dorsal hippocampus severely impaired behavioral performance in this task (Kim et al., 2012a). We also confirmed that the task using simple elemental cues, instead of scene stimuli, to association was not impaired by inactivation of the hippocampus (Lee et al., 2014). In addition, measuring CA1 cell activity in this task showed that the place cells modulated their activity according to the scene stimuli (Delcasso et al., 2014).

2. Anatomical connections of the CA1 and CA3

CA1 and CA3 are subregions of the hippocampus and are part of the trisynaptic circuit. Trisynaptic circuit is a circuit composed of perforant path from entorhinal cortex (EC) to dentate gyrus (DG), mossy fiber from dentate gyrus to CA3, and schaffer collateral from CA3 to CA1 (Andersen et al., 1969). In detail, the CA3 pyramidal cell receives three major inputs. First one is the mossy fiber from the DG granule cell. Mossy fiber input project particularly to the stratum lucidum of CA3 (Swanson et al., 1978; Claiborne et al., 1986). About 46 synapses of mossy fiber make a contact in one pyramidal cell in CA3 (Amaral et al., 1990), which is a small number compared to the other inputs, but each synapse is strong. Since the mossy fiber input from DG is sparse and strong, it was modeled as an input that can create a new representation in CA3 (Treves and Rolls, 1992). CA3 also received input from layer II of EC through the perforant path. The perforant path has synapses in the stratum lacunosum-moleculare of CA3 and there are about 3,600 synapses in one cell (Amaral et al., 1990), so it can be said that the number of synapses is much larger than that of mossy fibers, but the effect of individual synapses is relatively weak. The axons from the medial entorhinal cortex (MEC) and lateral entorhinal cortex (LEC) enter the deep and superficial part of stratum lacunosum-moleculare, respectively (Steward, 1976; Kerr et al., 2007). It was modeled as an input required for retrieval of representation stored in CA3 because it affects CA3 relatively

widely (Treves and Rolls, 1992). Lastly, there is a recurrent collateral, which is a connection between CA3 pyramidal cells. The synapse of the recurrent collateral is distributed in the stratum oriens and the stratum radiatum (Laurberg, 1979; Ishizuka et al., 1990). There are 12,000 synapses per cell, so it is the source of largest number of inputs (Amaral et al., 1990). The recurrent collateral is a unique anatomical feature of CA3, and it has been modeled that CA3 may function as autoassociative networks through recurrent collateral (Mcnaughton and Morris, 1987; Treves and Rolls, 1992; Rolls, 2007; Le Duigou et al., 2014).

CA1 receives the Schaffer collateral of CA3 in the stratum oriens and stratum radiatum (Laurberg, 1979; Ishizuka et al., 1990). In addition, layer III of EC input is also transmitted to the stratum lacunosum-moleculare through perforant path. In the CA1, the position of the synapse is divided along the transverse axis of the stratum lacunosum-moleculare depending on whether the axon is from MEC or LEC (Burwell, 2000; Kerr et al., 2007; Agster and Burwell, 2013). The axon of MEC is mainly located on the proximal part of the CA1 (close to the CA3) and the axon of LEC is located mainly on the distal part (close to the subiculum). In the MEC, several types of cells representing spatial information, such as head direction cell, border cell, and grid cell, have been reported (Hafting et al., 2005; Sargolini et al., 2006; Solstad et al., 2008). Whereas, cells in the LEC show poor spatial modulation (Hargreaves et al.,

2005) and are known to receive a lot of input from areas that process non-spatial information (Witter et al., 1989; Burwell and Amaral, 1998). Therefore, it has been suggested that the proximal part and distal part of CA1 play a segregated role in processing spatial and non-spatial information, respectively (Henriksen et al., 2010), due to this difference in distribution of perforant path. The subiculum is a major output structure of the CA1 and gives projection to both cortical and subcortical areas such as EC, retrosplenial cortex, lateral septum, nucleus accumbens, mammillary body, and anterior dorsal nucleus of thalamus (Kishi et al., 2000; Witter, 2006; Aggleton and Christiansen, 2015). The afferent of subiculum shows difference along the transverse axis, similar to the CA1. The distal part of CA1 projects to the proximal part of the subiculum (close to the CA1), and the proximal part of CA1 projects to the distal part of subiculum (close to the postsubiculum) (Amaral et al., 1991).

3. Properties of place cell activity

In 1971, O'Keefe and Dostrovsky first discovered a cell in the hippocampus firing at a specific location when the rat forages a space, which is "place cell" (O'Keefe and Dostrovsky, 1971). Their findings implied that the hippocampus represented the cognitive map (O'Keefe and Nadel, 1978), providing the physiological basis for the cognitive map theory suggested by Tolman (Tolman, 1948). After their discovery, a method of constructing a rate map was developed to quantitatively display the activity of the place cell. The measurements quantifying the characteristics of the rate map, such as spatial information score, sparsity, and coherence were also developed subsequently (Skaggs and McNaughton, 1993; Skaggs et al., 1996).

Since the discovery of the place cell, a lot of research has been conducted on how the place cell activity is affected by the surrounding environment. First, in 1987 Muller and Kubie reported that when the size or shape of the open field chamber where rats foraging changed the position of the place field unpredictably, and they called this phenomenon "remapping" (Muller and Kubie, 1987). When the environmental change is large, the place fields disappear, appear, or change their location, so they show a new representation which is completely unrelated to their original representation. Global remapping occurs not only by environmental changes but also by other factors. When the rat foraged in two visually identical chambers

which were connected by a corridor, the representation of place cells for two chambers were completely different (Skaggs and McNaughton, 1998; Tanila, 1999), which implied that the place cell activity is influenced by the experience or internal map of the animal, not only by the sensory input. In addition, it was reported that the place field on the linear track showed remapping according to the running direction (McNaughton et al., 1983; Barnes et al., 1990; Geva-Sagiv et al., 2016). In 2005, the presence of rate remapping was reported (Leutgeb et al., 2005), in which the location of the place field does not move and only the firing rate changes. Rate remapping appeared when there was a relatively small changes in the environment, such as changing the color of the chamber (Leutgeb et al., 2005; Fyhn et al., 2007). Rate remapping was interpreted as a coding scheme for representing an event and episodes at a specific location because only the firing rate of place cell changed without changing in location of place field (Leutgeb et al., 2005).

There has been consistent claim that place cells represent not only animal's location but also non-spatial information (Eichenbaum, 2000). In a continuous T-maze, when the rat performed an alternative choice task, it was reported that the activity of the place field on the stem part of the T-maze was modulated according to the turning side (Wood et al., 2000). There were other studies showing that the activity of the place cell was affected by the trajectory of the animal (Ferbinteanu and Shapiro, 2003; Catanese et al., 2014). Changing of

task demands also triggered remapping of the place cell (Markus et al., 1995; Hallock and Griffin, 2013). In the experiment of Markus and colleagues, the representation of place cells for the same chamber was dramatically changed when the reward site was changed from random to fixed locations. In addition, it has been reported that place cell activity is modulated by time (MacDonald et al., 2011) or tone frequency (Aronov et al., 2017). As such, it has been revealed that although the place cell is most affected by the location of the animal as in the initial discovery, they are also affected by the non-spatial factors as well.

Chapter 1. Visual scene representation of the CA1 and subiculum in the visual scene memory task

Introduction

The hippocampus is known to be important for remembering an episodic memory (Scoville and Milner, 1957; Zola-Morgan et al., 1986; Eichenbaum, 2000; Squire and Wixted, 2011) and for spatial navigation (O'Keefe and Dostrovsky, 1971; O'Keefe and Nadel, 1978; Moser et al., 2008). Recently, scene construction theory proposed how these two functions are possible in hippocampus (Hassabis and Maguire, 2007). Scene construction theory argues that the fundamental function of the hippocampus is scene processing. And because scene is an important component in remembering episodic memory or spatial navigation, the hippocampus involves in both functions (Maguire and Mullally, 2013).

In this respect, our laboratory considered a series of experiments to confirm this because we also considered that the scene processing is a key function of the hippocampus. In particular, our lab used a visual scene memory (VSM) task to control a visual scene stimulus seen by rats (Kim et al., 2012a). In this VSM task, rats were required to see a visual scene presented on the monitors at the end of T-maze and had to select the side associated with the scene (i.e., right or left) in order to get a reward. We found that inactivation of the dorsal hippocampus induces severe impairment on VSM task performance (Kim et al., 2012a; Lee et al., 2014). In addition, firing rate modulation that correlates with scene was observed when

measuring the activity of single neurons in the dorsal CA1 while rat performed this task (Delcasso et al., 2014). However, there was a difficulty to dissociate completely whether the rate modulation observed in CA1 got changed to a scene stimulus or a side of choices because there were only two scenes have used when one scene was associated to the left side and the other with the right side. Therefore, in this chapter of the thesis, I used four scenes so that two scenes can be associated with each side of choices. Through comparison between different scenes with the same choice side I expected to see how the hippocampal neurons respond to the visual scene without choice factor.

In the current study, I also recorded the single cell activities from the subiculum, which is a major output structure of the hippocampus. Anatomically, subiculum sits at an important position that might be suitable to send hippocampal information to other cortical areas (Witter et al., 2000; Witter et al., 2014). Therefore, I investigated not only representation of hippocampus for scene information, but also how this information is actually transmitted to other areas through the downstream structure. It has been reported that the subiculum showed different spatial representation compared to CA1 during rat forages in a chamber (Sharp, 1997, 1999). In addition, some types of spatial cells, like border cells (Lever et al., 2009) and axis cells (Olson et al., 2017) that fire along a specific axis of the track, were only observed in the dorsal subiculum, not in

CA1. Since these prior studies suggest the possibility of distinct information processing in the subiculum, I tested to see if subiculum is passively receiving a scene representation from CA1.

Materials and methods

Subjects

Seven male Long-Evans rats weighing 300–400 g were used. Food was restricted to maintain body weight at 85% of free-feeding weight, and water was available ad libitum. Animals were housed individually under a 12-h light/dark cycle. All protocols used are in compliance with the Institutional Animal Care and Use Committee of Seoul National University.

Behavioral apparatus

An elevated, T-shaped linear track (47 x 8 cm stem for one rat and 73 x 8 cm stem for others with two 38 x 8 cm arms) containing a food well (2.5 cm in diameter and 0.8 cm deep) at the end of each arm was used in the visual scene memory (VSM) task (**Figure 1**). A guillotine door-operated start box (22.5 x 16 x 31.5 cm) was attached at the bottom of the stem. Three LCD monitors were installed as an array surrounding the upper portion of the track to display visual scene stimuli. Four optic fiber sensors (Autonics, Korea) were installed along the track at a distance 1, 27, 47 and 67 cm from the entrance of the start box to detect the animal's position and to control the onset and offset of scenes. Additional optic sensors were installed inside food wells to record the moment the rat obtained the reward. Sensor activity was transmitted to a data-acquisition system (Digital Lynx SX, Neuralynx) as TTL signal. I used custom-written software

created in MATLAB (MathWorks) and Psychtoolbox to control scene stimuli and transmit TTL signals associated with trial information (e.g., scene stimuli, choice accuracy) to the data-acquisition system. The experimental room was dimly lit by a ceiling lamp. A digital camera attached to the ceiling recorded both positions and directions of the animal's head at a sampling rate of 30 Hz. Black curtains surrounded the apparatus, and white noise was played by two loudspeakers (80 dB) during behavioral sessions to mask unwanted environmental noise.

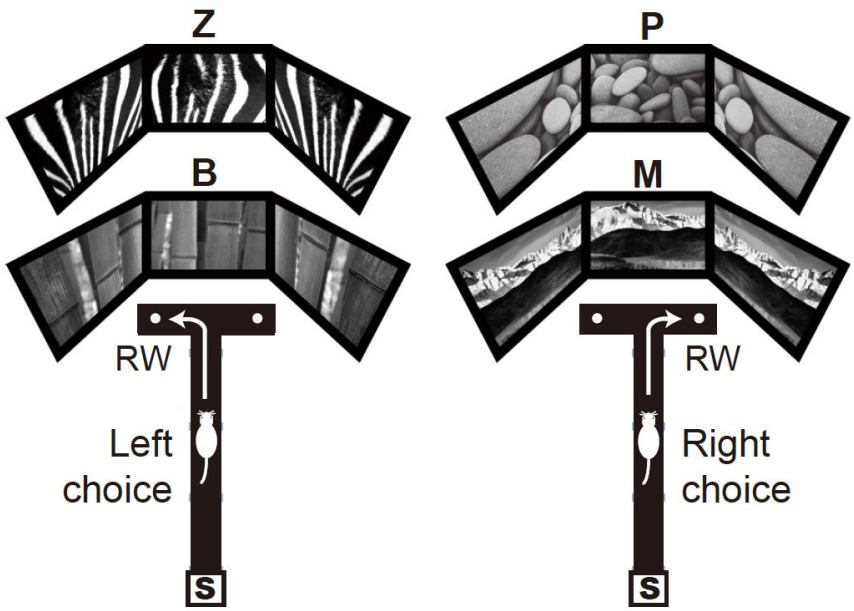

Figure 1. Visual scene memory task. An elevated, T-shaped linear track was used in the visual scene memory task. Three LCD monitors were installed as an array surrounding the track to display visual scene stimuli. Four grayscale visual patterns (Z: zebra stripes, P: pebbles, B: bamboo, M: mountains) were used as scene stimuli. Rats were required to choose correct side associated with the presented visual scene. Zebra stripes and bamboo patterns were associated with the left food well, and pebbles and mountain patterns were associated with the right food well. RW: reward, S: start box.

Visual scene memory (VSM) task

In the VMS task, the experimenter started a trial by opening the door of the start box. This opening was detected by the optical sensor, immediately triggering the display of the visual scenes on the monitors. The rat ran along the track toward the end of the stem to choose either the left or right arm in association with the visual scene (**Figure 1**). The food well in the arm that was correctly associated with the scene contained a quarter piece of cereal reward (Froot Loops, Kellogg's), and the rat obtained the reward by displacing a black acrylic disk covering the food well. If the rat made an incorrect choice, no reward was provided, and the rat was gently guided back to the start box immediately after the incorrect choice was made. An inter-trial interval (10 s) was given after a correct trial; a longer (20 s) inter-trial interval was applied after an incorrect choice was made. The experimenter placed a reward in one of the food wells for the next trial (following the pre-determined baiting sequence) during the intertrial interval. The rat was confined in the start box during the intertrial interval, and the high walls (31.5 cm) and background white noise (80 dB) in the room made it difficult for the rat to discern the next trial's baited food-well location from the start box.

Four grayscale visual patterns (zebra stripes, pebbles, bamboo, and snow-covered mountains) were used as scene stimuli. The visual scenes were equalized for luminance (set at an average intensity value = 103 in Adobe Photoshop). For all trials, zebra stripes and

bamboo patterns were associated with the left food well, and pebbles and mountain patterns were associated with the food well in the right arm (**Figure 1**). Rats were initially trained to criteria with a pair of visual scenes (≥75% correct choices for each scene for two consecutive days) and then were trained with the second pair of scenes. The training order for the use of different scene pairs was counterbalanced among the rats. Forty trials were given in a pre-surgical training session. The presentation sequence of scene stimuli across trials in a given session was pseudo-randomized with the following constraints: 1) each scene was presented equally in every 20 trials, and 2) the same food well was not used for rewards in four consecutive trials. Once rats learned both pairs of scene stimuli according to criterion (≥75% correct choices for all scenes for two consecutive days; **Figure 2**), a hyperdrive was implanted.

Surgery

After behavioral training, a hyperdrive carrying 24 tetrodes and 3 reference electrodes was implanted for recording single-unit spiking activities simultaneously from the dorsal CA1 and subiculum. The impedance of each tetrode was adjusted to 100–300 kΩ (measured in gold solution at 1 kHz with an impedance tester) 1 day before the hyperdrive was implanted. For surgery, the rat was anesthetized with an intraperitoneal injection of sodium pentobarbital (Nembutal, 65 mg/kg) and its head was fixed in the stereotaxic frame (Kopf

Instruments, USA). Inhalation of isoflurane (0.5-2% isoflurane mixed with 100% oxygen) was used to maintain the anesthesia throughout surgery afterwards. Before making an incision along the longitudinal midline of the scalp, the scalpel blade and the incision area was sprayed with benzocaine for local anesthesia. A burr hole was drilled into the skull on the right hemisphere to insert the bundle of the hyperdrive. The target coordinates for implantation was pre-determined to allow the tetrodes to cover a range from 3.48 to 6.6 mm posterior to bregma and from 1 to 3 mm lateral to the midline. Then, the hyperdrive was chronically affixed to the skull by applying bone cement to its bundle and multiple skull screws near the bundle. After surgery, ibuprofen syrup was orally administered to control the animal's general pain and the rat was left in a veterinary intensive care unit in which temperature and humidity were strictly controlled. More detailed surgical procedures can be found in our previous studies (Delcasso et al., 2014; Ahn and Lee, 2015).

Electrophysiology recording

After a week of recovery from surgery, rats were re-trained (~160 trials per session using the same pairs of scenes used before surgery) until they showed stable performance ($\geq$ 75% correct choices for each scene); over the course of a number of days during this period, tetrodes were gradually lowered into target areas. For tetrode adjustments, each rat was placed on a pedestal in a custom-made

aluminum booth outside the behavioral testing room, and the adjustment of tetrodes began (Ahn et al., 2019). Neural signals were transmitted through the headstage (HS-36, Neuralynx) and tether attached to the electrode interface board of the hyperdrive to the data-acquisition system. Neural signals were digitized at 32 kHz (filtered at 600–6,000 Hz) and amplified 1000–10,000 times. Tetrodes were lowered daily by small increments to reach the target areas and to maximize the number of single units recorded per tetrode.

The behavioral paradigm for recording sessions

Once the main electrophysiology recording session began, all four scenes shown during the training period were presented in an intermixed fashion within a session (~160 trials per session). During the behavioral task, neural signals were relayed through a slip-ring commutator to the data-acquisition system, and an array of green and red LEDs was attached to the headstage to monitor the animal's positions and head directions using a ceiling camera (sampling rate 30 Hz).

Histology

After the completion of all recording sessions, an electrolytic lesion was made via each tetrode (10 μA current for 10 s) to mark the tip position. After 24 hours, the rat inhaled an overdose of CO_2 and was perfused transcardially, first with phosphate-buffered saline and then

with a 4% v/v formaldehyde solution. The brain was extracted and soaked in 4% v/v formaldehyde-30% sucrose solution at 4°C until it sank to the bottom of the container. After post-fixation procedures, the brain was gelatin-coated and soaked in 4% v/v formaldehyde-30% sucrose solution. The brain was sectioned at 30-40 μm using a freezing microtome (HM 430; Thermo-Fisher Scientific), after which sections were mounted and stained with thionin. Photomicrographs of brain tissues were taken using a digital camera (Eclipse 80i, Nikon) attached to a microscope, and were reconstructed three-dimensionally to match the configuration of the tetrodes from the initial bundle design. The exact locations of tetrodes were determined using the 3D reconstructed images and physiological depth profiles recorded at the time of data acquisition. To better present tetrode positions, I constructed a flat map of the dorsal CA1 and subiculum using Nissl-stained coronal sections and marked the tetrode positions in all rats in the flat map.

Construction of a flat map

A flat map was constructed using the coronal brain sections from all rats (**Figure 3A**). Nissl-stained sections were aligned to orient tetrode tracks vertically, and the length of the cell layer in the subiculum and CA1 of each section was measured using Image J software. Because the cell layer was curved along the transverse axis, multiple dots were first marked along the cell layer at narrow

intervals, and the distance between the dots was calculated by summing their x and y positions. The marking procedures for dots started from the most distal end of the subiculum or CA1 and proceeded toward the proximal border. The lateral border of the flat map was based on the measured lengths of cell layers along the anterior-posterior axis. Because of individual differences in brain sizes and sectioning angles among rats, flat maps for all rats were proportionally adjusted by using the medial habenular nucleus and superior colliculus as references (Paxinos and Watson, 2009). After normalizing along the anterior-posterior axis, the length of the cell layer was finally determined by taking the median value of distances measured for all rats. The relative tetrode tip positions were then marked on the flat map.

Unit isolation

Single units were simultaneously recorded from the dorsal CA1 (n = 364) and dorsal subiculum (n = 320), and were isolated manually using both commercial (SpikeSort3D, Neuralynx) and custom-written software (WinClust) using multiple waveform parameters, including peak and energy, as previously described (Lee and Kim, 2010; Delcasso et al., 2014). Neurons that did not satisfy the following set of criteria were excluded in further analysis: (i) average peak-to-valley amplitude of waveforms $\geq$ 75 μV (79 units excluded), (ii) proportion of spikes within a 1-ms refractory period < 1% of total

spikes (5 units excluded) and (iii) average firing rate during the outbound journey on the stem ≥ 1 Hz (174 units excluded). In addition, fast-spiking neurons (mean firing rate ≥ 10 Hz; width of the average waveform < 325 μs) were excluded (n = 55) from the analysis. Only those units that met the above criteria (n = 129 in CA1, n = 242 in subiculum) were used for final analysis. The reason behind the larger amount of neurons being filtered out in CA1 (n = 133) than in the subiculum (n = 41) was largely because many cells (approximately half of the isolated clusters) fired sparsely during the outbound journey in CA1, showing lower firing rates (< 1Hz), but that was not the case in the subiculum.

Data analysis

Characterizing basic firing properties

To measure the amount of spatial information conveyed by a unit, I constructed a linearized spatial rate map. Position data from behavioral sessions were scaled down (bin size = 4 cm^2). Then, a raw spatial rate map was constructed by dividing the number of spikes by the duration of visit for each bin. The spatial rate maps were smoothed by moving average method for illustration purpose only. Spatial information was computed according to the following equation (Skaggs and McNaughton, 1993):

$$\text{Spatial information score (bits/spike)} = \sum_i p_i \frac{\lambda_i}{\lambda} \log_2 \frac{\lambda_i}{\lambda}$$

, where i denotes bin, p_i is occupancy rate in the ith bin, λ_i is the mean firing rate in the ith bin, and λ is the overall mean firing rate. The mean firing rate of a unit was obtained by averaging the firing rates in the raw rate map. Other conventional spatial firing characteristics of cells such as spatial selectivity and sparsity measures were computed using the following formula (Skaggs et al., 1996):

$$\text{Sparsity} = \frac{(\sum p_i \lambda_i)^2}{(\sum p_i \lambda_i^2)}$$

$$\text{Selectivity} = \frac{\max(\lambda_i)}{\lambda}$$

, where the same symbols were used as in the formula for calculating spatial information above. To minimize the effect of animal's behavior on the measurements, I assumed that p_i in the sparsity formulas had uniform distribution on the maze (Jung et al., 1994). Coherence of a place field was computed as z-transforms of correlations between two lists of spatial firing rates (i.e., the firing rate of each spatial bin and average firing rate of each bin's nearest bins) (Muller and Kubie, 1989). Following the previous study (Kim et al., 2012b), a burst index was defined as the power of autocorrelation during 1-6 ms normalized by the power during 1-20 ms.

Construction of an event rate map

I designated seven sequential task-relevant events as follows: trial

start (opening of the door of the start box), three different time points detected by the optic sensors installed along the stem, spatial choice (turning to either the left or right arm), reaching the half point between the moment of spatial choice and reaching the arm end, and displacing the disc overlying the food well that contained reward (**Figure 5A**). Timestamps for individual events were recorded by optic sensors, except for the choice event. Timestamps for the choice event were determined by detecting the spatial bin in which a significant difference between position traces associated with the left and right choice trials (two-sample t-test). The duration of individual events across trials were normalized and were split into three bins. Then, a raw event rate map (ERM) was constructed by dividing the number of spikes by the duration of occupancy for each bin (**Figure 5B**). The raw ERM was smoothed using a moving average method to define field boundaries and for illustration purposes. However, all data analysis was conducted using raw ERMs.

Boundaries and categorization of event fields

ERMs were categorized into three groups based on the number of firing fields; single field (SF), multiple fields (MF) and event-unrelated fields (**Figures 7A** and **7B**). If the minimum firing rate of an ERM was larger than the half maximal firing rate, the rate map was classified as an event-unrelated field and the event-unrelated fields were excluded in the following analysis. The directions of

change in firing rates across the events were measured by comparing the firing rates before and after the events to determine the boundaries of a field. That is, the firing rate of a bin was statistically compared with the firing rate in the next bin (using Wilcoxon rank-sum test) in an ERM to determine the direction of firing-rate changes (i.e., increase, decrease, and no change). The sequence of the changing direction in firing rate across the events made it possible to define local minima. Within the local minima, the bin with the maximal firing rate was defined as the peak of the field, and the boundaries were defined by detecting the bins in which the firing rates decreased to less than 40% of the peak firing rate. If there was no bin with the firing rate lower than the criteria, the local minimum became a field boundary. After defining the boundaries, cells were classified into two types: that is, a single field (SF) and multiple fields (MF) based on the number of the fields. A field with a ratio of the minimum to maximum firing rates exceeding 0.5 was not considered as a valid field. Field width was measured by counting the number of bins between the boundaries of a field. If there were more than one field in a rate map (i.e., MF), then each field was treated as independent fields.

Autocorrelation matrix

An autocorrelation matrix was constructed for the cells with single fields (Gothard et al., 1996; Lee et al., 2004) to measure the

representation of the task period at the neural population level (**Figure 8B**). For this purpose, first, a population rate map consisted of the individual rate maps (each normalized by the cell's maximum firing rate) was prepared, and the correlation between the two vectors from the same population rate map was computed using the following equation for obtaining the Pearson correlation coefficient:

$$R_{ij} = \frac{\sum_{C=1}^{n}(FR_{i,C} - \overline{FR}_i)(FR_{j,C} - \overline{FR}_j)}{\sqrt{\sum_{C=1}^{n}(FR_{i,C} - \overline{FR}_i)^2}\sqrt{\sum_{C=1}^{n}(FR_{j,C} - \overline{FR}_j)^2}}$$

where *i* and *j* denote the population vector from the population rate map, *n* is the number of cells, *C* indicates *C*-th cell in the population, *FR* is the firing rate of the cell, and $\overline{FR}$ is the mean firing rate of the vector. As a result, a symmetric matrix was obtained, and the matrix space was then divided into task-congruent (TC) and task-incongruent (TI) sections (**Figure 8C**). Specifically, the task-congruent area denotes the subregion of the correlation matrix in which the correlation coefficients were calculated between the same task epochs (e.g., between pre-choice and pre-choice epochs), and the task-incongruent area represents the region in which the correlation coefficients were obtained between different task epochs (e.g., between pre-choice and post-choice epochs). Then, the correlation coefficients associated with the two areas were statistically compared using the Wilcoxon rank-sum test.

Procedures for random shifting of ERM

The locations of individual firing fields in the population ERM were shuffled while the sizes of individual fields were maintained. Specifically, the ERMs of individual cells were shifted by random amounts of bins in either forward or backward direction, and the resulting ERMs were realigned (**Figure 9A**). The range of shifting was restricted so that the individual field boundaries did not exceed the boundaries of the population ERM after shifting. To compare the effects of the random shifting of individual fields both in the CA1 and subiculum, I measured the similarity of the resulting autocorrelation matrix (**Figure 9B**) with the original autocorrelation matrix (**Figure 8B**) by calculating a Pearson correlation coefficient. Then, the shifting procedure was repeated for 1000 times, and the Pearson correlation coefficient was calculated each time using the original autocorrelation matrix as a counterpart. The resulting distributions of correlation coefficients were compared by a Wilcoxon rank-sum test in the CA1 and subiculum.

Speed analysis

The rat's positions were recorded at 30 Hz in the current study. I divided the length of the three consecutive points by the duration of time to calculate the instantaneous running speed, and assigned the speed value to the middle point of the three. For constructing the speed map of a session, the instantaneous running speeds were

averaged for each event bin as when constructing an ERM. The speed map before the track entrance event was not available because the matching position data were not sampled inside the start box in the current experimental setup. Then, I defined that a cell's firing pattern was speed-correlated when the following criteria were met: (i) the Pearson correlation coefficient calculated between the speed map and ERM was both positive and statistically significant, and (ii) the Pearson correlation coefficient between the in-field firing rate for each trial and its associated speed was both positive and significant. For calculating the in-field firing rate or the in-field running speed, only the data obtained before the choice event were used because the running speeds were systematically different between the two arms.

Rate difference index (RDI)

I obtained an RDI to measure the amount of rate modulation between two rate maps by calculating an absolute value of Cohen's d:

$$\text{Rate difference index (RDI)} = \left|\frac{mean(FR_1) - mean(FR_2)}{std(FR_1, FR_2)}\right|$$

, where FR_1 and FR_2 denote the in-field firing rates of the trials associated with two different conditions, respectively. Since the Cohen's d measure is a standardized measure that includes a term for standard deviation in the denominator, a possible confounding effect induced by the variability in intrinsic firing should be controlled in this analysis. The difference in firing rates between the left and right choice trials was computed as RDI_{CHOICE} (**Figure 12A**). RDI_{SCN} was

calculated as the difference of the two rate maps associated with different scenes that shared the same choice response (e.g., $RDI_{SCN\text{-}L}$ for the zebra-bamboo scene pair and $RDI_{SCN\text{-}R}$ for the pebbles-mountain pair; the bigger of the two taken) (**Figure 12B**).

Experimental design and statistical analysis

Seven male Long-Evans rats were used in the VSM task (29 sessions in total). Two sessions were excluded because of the malfunctioning optic sensors. Neural spiking data were analyzed using nonparametric statistics and a Bonferroni correction procedure was used during post-hoc tests involving multiple comparisons. Testing for statistical significance was two-sided, except when testing significance against known criteria (e.g., behavior performance criterion of 75% or chance performance level of 50%). The level of statistical significance was set at $\alpha = 0.05$ unless noted otherwise. Behavioral performance levels for different scene stimuli were compared using a repeated-measures ANOVA (paired t-test for post-hoc analysis). A one-sample t-test was used to compare performance against the performance criterion. Comparisons of basic firing properties and field size between two regions (e.g., CA1 and subiculum) were conducted using a Wilcoxon rank-sum test. A Pearson's chi-square test was used to compare the proportions of cell types in the CA1 and subiculum. The Wilcoxon rank-sum test was used to compare RDI_{CHOICE}, RDI_{SCN} between two regions.

Results

Simultaneous recording of single units from the CA1 and subiculum in the VSM task

Single units were recorded simultaneously from both the CA1 and subiculum while rats performed the VSM task in which four visual scenes were presented in a pseudo-random sequence on three adjacent monitors surrounding the T-maze (**Figure 1**). The rat was required to choose either the left or the right arm associated with a given visual scene. By the time when the main recording session began, all rats made correct choices in more than 85% of the trials for all scene stimuli, and performance for all scenes exceeded the criterion of 75% (P-values < 0.0001, one-sample t-test) (**Figure 2**).

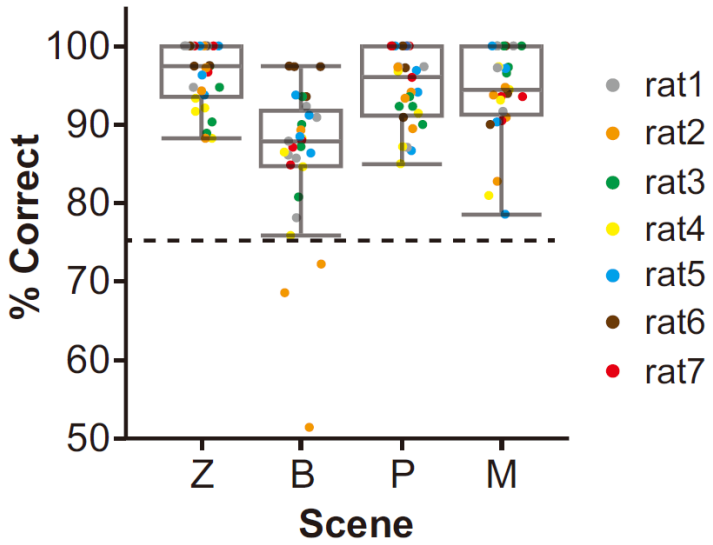

Figure 2. Behavioral performance in VSM task. Performance for each scene stimulus were plotted as box plots. Rats were separately marked by color. Overall performances exceeded criterion (dashed line, 75%) for all scenes. Box plot indicates range and median value.

I reconstructed the locations of tetrode tips on a flat map (**Figure 3A**), using both histological results (**Figure 3B**) and physiological recording profiles. The recording locations were distributed approximately 3.5 to 6.6 mm posterior to bregma. The units that satisfied the unit-isolation criteria (n = 129 in CA1; n = 242 in subiculum) were found along the entire proximodistal axis in both CA1 and subiculum although more CA1 units were recorded in the proximal portion than in the distal part. There was a narrow zone at the border between the distal CA1 and the proximal subiculum where cell layers of both regions overlapped (SUB/CA1 in **Figure 3A** and **3B**). I assigned the units recorded from this region to either CA1 or subiculum using multiple criteria, including (a) the baseline firing rate recorded in the start box in the absence of the scene stimulus (< 1 Hz in the CA1 and > 4 Hz in the subiculum), (b) the morphological characteristics of the cell layers in Nissl-stained sections, and (c) the depth-profiles for individual electrodes recorded during the tetrode-adjustment period. As reported in prior studies (Barnes et al., 1990; Sharp and Green, 1994; Kim et al., 2012b), the mean firing rate was higher on average in the subiculum than in the CA1 (Z = 6.83, p < 0.0001, Wilcoxon rank-sum test) (**Figure 4**). In addition, units recorded from the CA1 bursted more (Z = 12.91, p < 0.0001, Wilcoxon rank-sum test) and fired more spatially (spatial information score: 1.12 ± 0.06 in CA1, 0.25 ± 0.02 in subiculum; sparsity: 0.43 ± 0.02 in CA1, 0.78 ± 0.01 in subiculum; coherence: 1.81 ± 0.05 in

CA1, 1.34 ± 0.04 in subiculum; spatial selectivity: 4.34 ± 0.18 in CA1, 2.14 ± 0.07 in subiculum; Mean ± S.E.M.; P-values < 0.0001, Wilcoxon rank-sum test) than the units recorded from the subiculum (**Figure 4**).

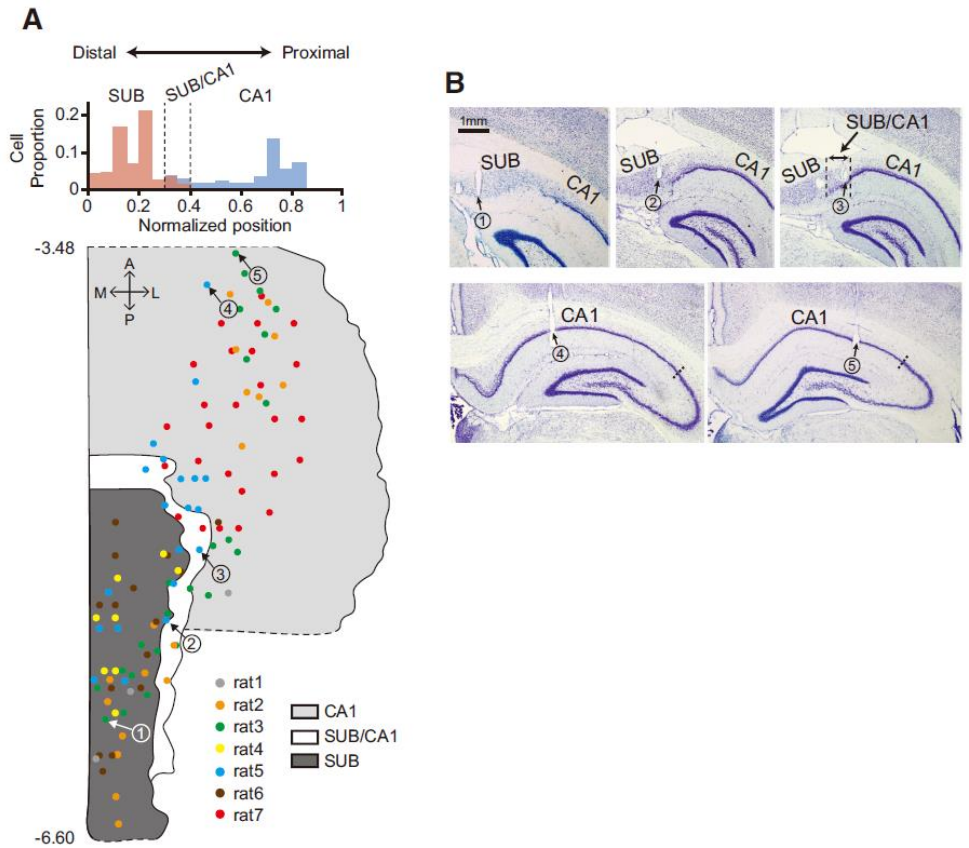

Figure 3. Simultaneous recording of single units from the CA1 and subiculum. (**A**) Proportional distribution of cells recorded in the CA1 (blue) and subiculum (SUB; red) along the proximo-distal axis (top) and a flat map showing tetrode positions in the CA1 and subiculum (bottom). The intermediate transition zone (SUB/CA1) is colored in white. Numbers on the left of the flat map indicate relative positions (mm) from bregma. Colored-dots represent tetrode positions for individual rats. A: anterior, P: posterior, M: medial, L: lateral. (**B**) Nissl-stained photomicrographs of the tissue sections that contained the tetrode trajectories marked by the arrows in (A).

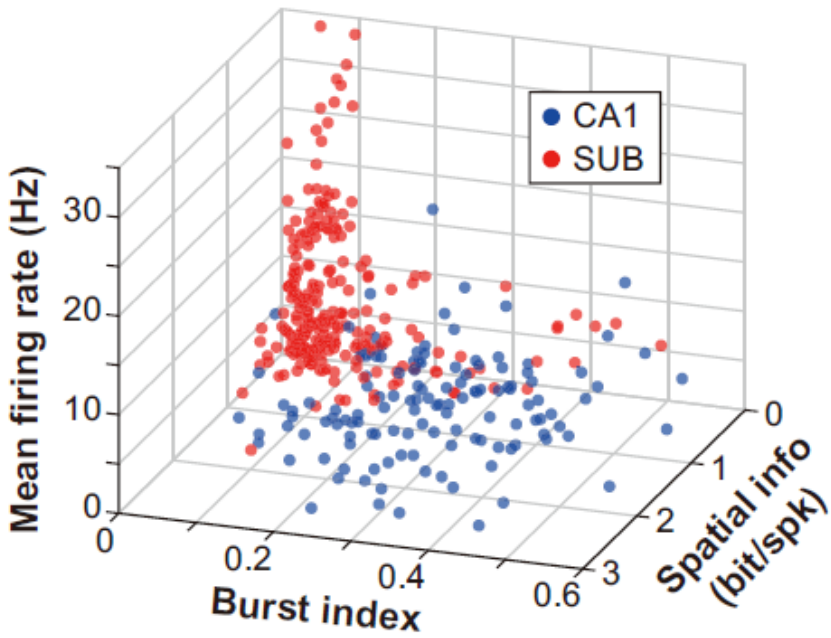

Figure 4. Basic firing properties of CA1 and subiculum. Mean firing rate, burst index and spatial information score of single neurons in the CA1 (blue dots) and subiculum (red dots) were plotted in 3-D graph. CA1 cells had higher spatial information score and burst index, whereas subiculum cells had higher mean firing rate.

Neurons in the CA1 and subiculum responded to task-relevant events

In the current experiment, although I recorded both neural activity and video data of rat's location simultaneously, the video signal was not acquired for inside the start box because of technical issue. Therefore, I needed an alternative method for analyzing neural activity in temporal dimension rather than spatial dimension to not lose the data inside the start box. Furthermore, the choice point is cognitively important event in this task. Since the memory demand gets lower after the rat choose left or right arm at the intersection, the neural activity was needed to examined separately according to the choice point. However, the location of choice on the track was variable across session, so it was hard to analyze neural activity all together based on spatial rate map. Therefore, I decided to organize the neural firing patterns by using the critical events that occurred in the task (Aronov et al., 2017), instead of using location-based neural representations. I named such a neural representation "event rate map (ERM)". To construct an ERM, I defined three critical events associated with task demands as follows: (a) 'S' - opening of the door of the start box (which also corresponded to the onset of the scene stimulus, detected online by an optic sensor), (b) 'C' – choosing the left or right arm at the intersection (detected offline by calculating the position-diverging point), and (c) 'R' - displacing the disc that covered the food well containing reward (detected online by optic

sensors) (**Figure 5A**). I also used the activities from three additional sensors and the bisecting point between the choice point and reward location as minor events to construct individual ERMs. Therefore, an ERM is composed of seven time points associated with the abovementioned seven events and the six event epochs between those time points (**Figure 5B**). Constructing an ERM enabled me to analyze the neural firing patterns recorded immediately before and after the door-opening event in the start box (which coincided with the onset of a scene stimulus) while capturing the spatial firing characteristics at the same time (**Figure 6**).

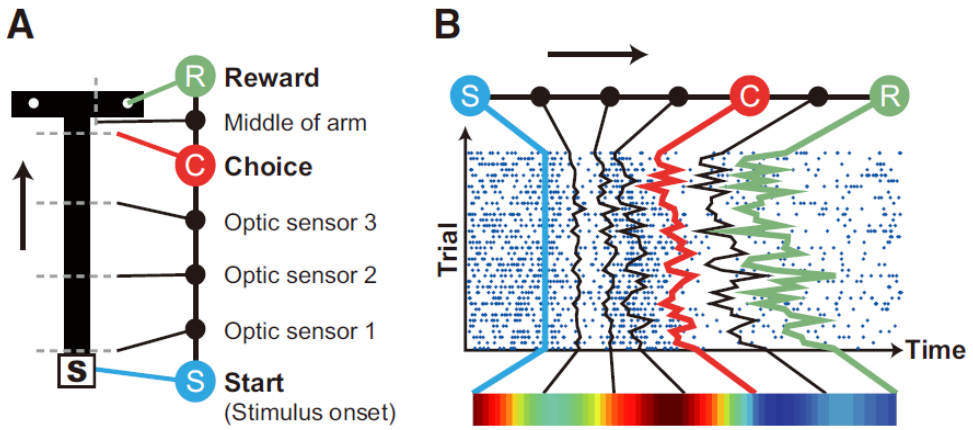

Figure 5. Construction of event rate map (ERM). (**A**) Major events in the VSM task. The opening of the start box door (S), turning to the left or right arm at the choice point (C), and reaching the reward location (R) were defined as three major events. Three sensor-crossing points in the stem and bisecting point of each arm were minor events. The arrow denotes the running direction. (**B**) Event rate map (ERM). The raster plot of a single unit is used to as an example to illustrate how spiking activities were grouped into discrete event epochs to result in the ERM.

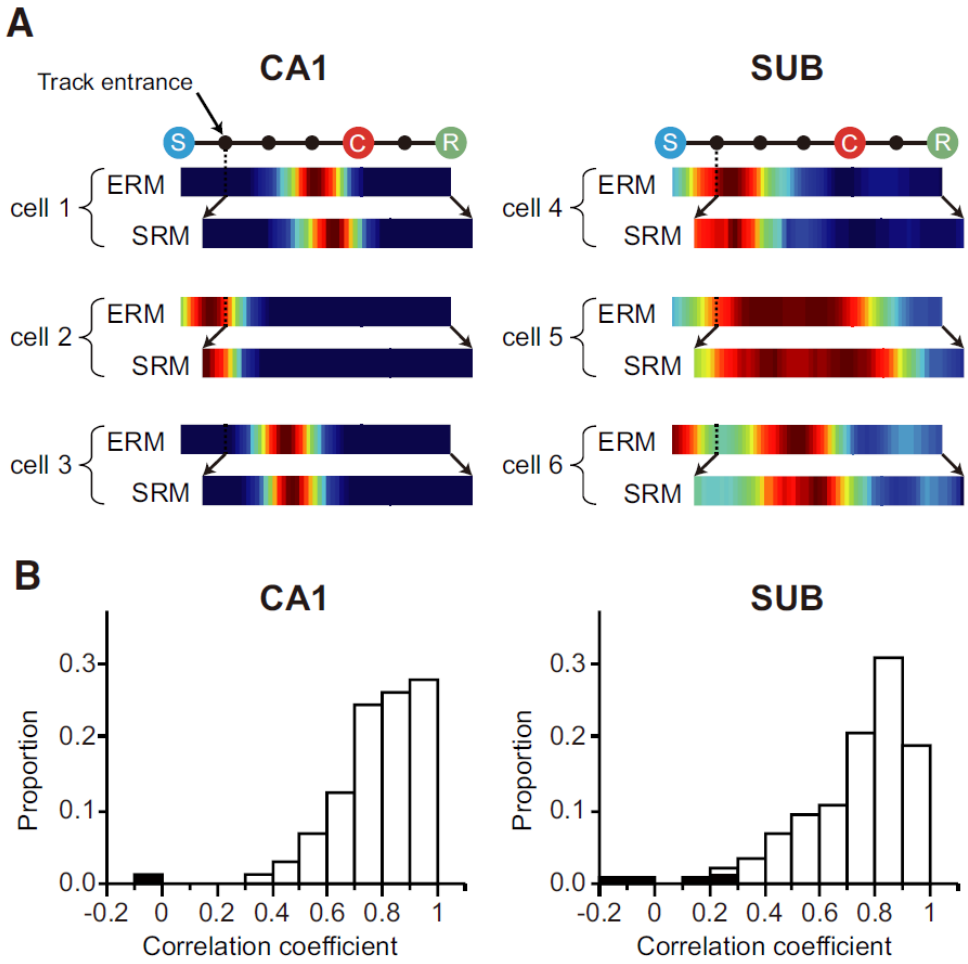

Figure 6. High correlation between ERM and SRM (**A**) Examples of the event rate maps (ERM) and spatial rate maps (SRM) of cells in the CA1 and subiculum. The epoch between the opening of the start box and track entrance was not represented in the spatial rate map because the associated position data were not recorded in the start box in the experimental settings, whereas the event rate map could represent neural activity in the entire task period (including the neural activity inside the start box). Although the information-organizing schemes were different between the event rate map (time)

and spatial rate map (location), both formats were very similar because time and location were highly correlated in the current task on the maze. (**B**) Distribution of the Pearson correlation coefficients between the event rate maps and spatial rate maps (excluding the start box) of individual neurons of the CA1 (left) and subiculum (right). Two type of maps were highly correlated in the most of cells, and only 6 out of 325 cells (n = 1/109 in CA1, n = 5/216 in subiculum) showed no correlation between two maps.

Examining the individual ERMs of the CA1 and subiculum showed some differences between the two areas. Specifically, most units in the CA1 showed a single field occupying a narrow zone seemingly corresponding to the size of a single event epoch in the ERM ('SF' in **Figure 7A**). Some units fired at multiple epochs in the ERM in the CA1 ('MF' in **Figure 7A**) although there were not many such cases. In contrast, subicular units tended to fire across contiguous epochs in the ERM, resulting in longer single firing fields ('SF' in **Figure 7B**) or, when firing in multiple epochs separated from each other, multiple firing fields ('MF' in **Figure 7B**). In some units, I could not detect event-related fields (event-unrelated units; see Materials and Methods) and I excluded those units for analysis. Most CA1 units showed single fields (> 80%), whereas the units exhibiting single fields and multiple fields were almost equally found in the subiculum ($\chi^2_{(1)} = 49.69$, $p < 0.001$, Chi-square test) (**Figure 7C**). The sizes of event-related fields in the CA1 and subiculum were also statistically different from each other ($\chi^2_{(2)} = 75.92$, $p < 0.0001$, Kruskal-Wallis test; inset in **Figure 7D**). Specifically, the size of single fields in the CA1 was significantly smaller than that of the single fields in the subiculum (SF: $Z = 8.09$, $p < 0.0001$; single fields within MF: $Z = 2.63$, $p < 0.01$; Wilcoxon rank-sum test), and single fields in the subiculum were larger than the individual fields of the multiple fields in the subiculum ($Z = 7.27$, $p < 0.0001$).

Interestingly, the proximal region of the subiculum contained

more multiple-field units than single-field units and vice versa in the distal subiculum (Z = 2.16, p = 0.033, Wilcoxon rank-sum test) (**Figure 7E**). These might be attributable to the fact that the distal portion of the subiculum receives stronger inputs from the medial entorhinal cortex, whereas the proximal subiculum receives more inputs from the lateral entorhinal cortex (Cembrowski et al., 2018).

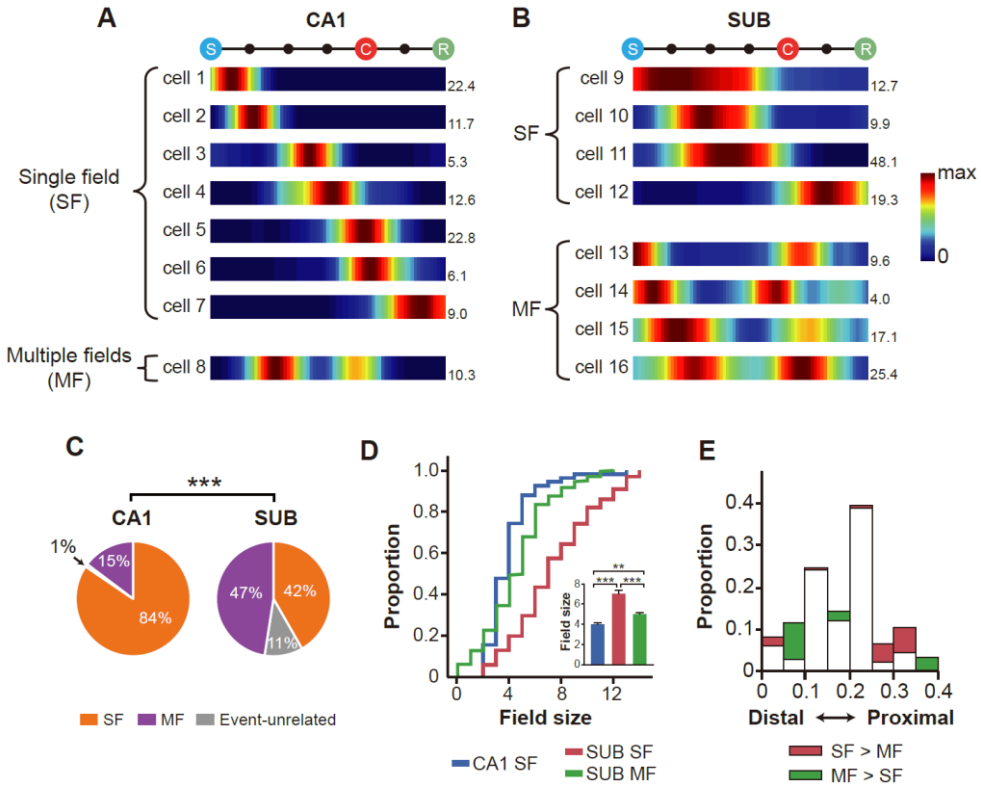

Figure 7. Types of firing fields in the CA1 and subiculum. (**A** and **B**) Representative ERMs in the CA1 (A) and subiculum (B). Numbers indicate the maximal firing rates. The color bar denotes the color scale for firing rate (max: maximal firing rate). (**C**) The proportion of single- and multiple-field types in the CA1 and subiculum. (**D**) Comparison of the field sizes of the units with single fields and multiple fields in the CA1 and subiculum. Inset: Same data presented as bar graphs. Median ± 95% confidence interval/2. $^{**}p < 0.01$, $^{***}p < 0.001$. (**E**) Histograms to compare the proximo-distal distributions of single-field units with multiple-field units in the subiculum. Overlapping areas between single- and multiple-field distributions are colored in white. Note the presence of more multiple-field units in the distal subiculum (green areas) and more single-field units in the proximal subiculum (red areas).

Neural populations in the subiculum fired schematically, capturing the task structure better than those in the CA1

To examine the information structure conveyed by the neural populations in the subiculum, I constructed a population ERM by combining all the individual ERMs (aligned according to their maximal firing locations along the entire task period) both for the CA1 and subiculum (**Figure 8A**). Because the relative lack of the units showing multiple fields in the CA1, only the units whose ERMs showed single fields were analyzed in both CA1 and subiculum. As expected from the individual ERMs, event-related fields covering individual epochs were linearly aligned from the trial start (S) to goal-reaching (R) event in the neural population in the CA1. In contrast, individual fields were wider in the population ERM in the subiculum, particularly in the periods starting from the start box opening (S) to the spatial choice (C), and from the spatial choice (C) to the reward location (R).

I then computed an autocorrelation matrix by cross-correlating the population ERM with itself to show the amount of correlation in the population firing patterns between different event periods (**Figure 8B**). There was a narrow, high correlation band (seemingly matching the size of an event epoch in the ERM) along the diagonal in the CA1. However, in the subiculum, the autocorrelation matrix clearly showed two rectangular, high-correlation regions (i.e., task-congruent regions) corresponding to

the pre-choice and post-choice epochs of the task. Furthermore, the correlation was relatively lower in the areas where the population rate maps in the pre-choice period were correlated with those in the post-choice period, and vice versa (i.e., task-incongruent region). It appears that the neural population in the subiculum "schematically" represented the most critical two epochs of the task; that is, the pre-choice (from stimulus onset to choice) and post-choice (from choice to reward) epochs in a given trial. The average amount of correlation in the task-congruent regions (orange triangular areas in **Figure 8C**) in the autocorrelation matrix was greater in the subiculum than in the CA1 ($Z = 4.30$, $p < 0.0001$, Wilcoxon rank-sum test; **Figure 8D**). In contrast, the correlation was significantly lower in the task-incongruent area (blue rectangular area in **Figure 8C**) in the subiculum than in the CA1 ($Z = 3.85$, $p < 0.0001$, Wilcoxon rank-sum test; **Figure 8E**).

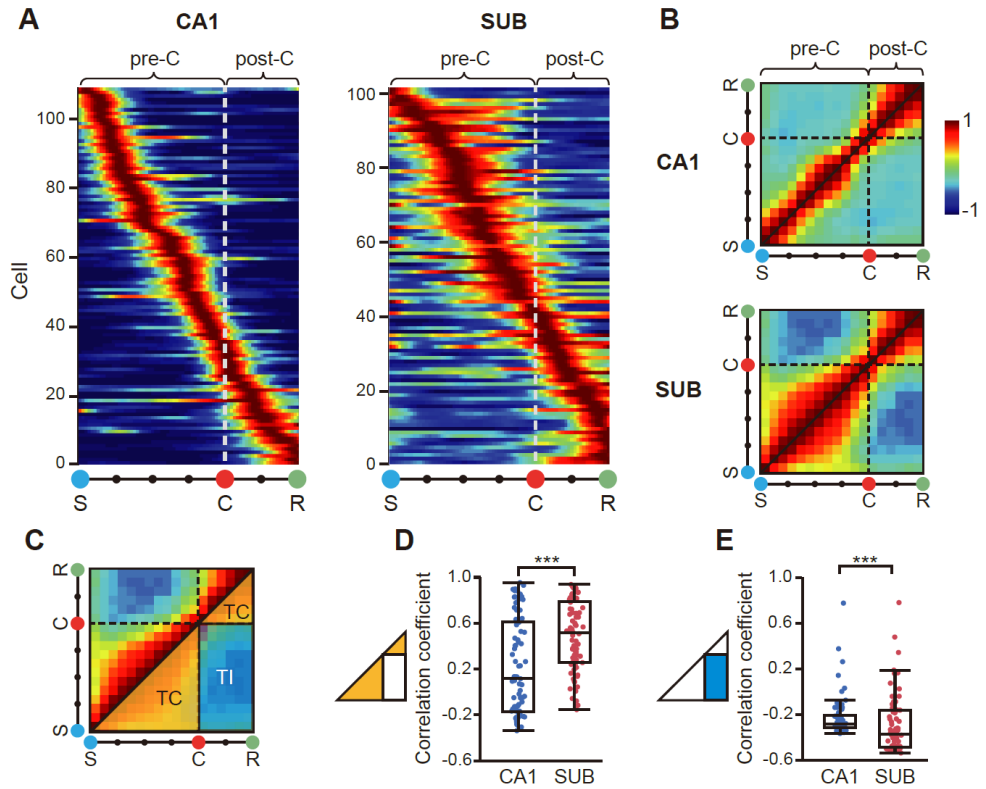

Figure 8. Schematic firing patterns of the neural populations in the subiculum, but not in the CA1. (**A**) Population ERMs for the CA1 and subiculum. Individual ERMs were aligned according to their maximal firing locations along the event dimension (S-C-R). The white dotted line denotes the boundary between the pre-choice (pre-C: S to C) and post-choice (post-C: C to R) periods. (**B**) Autocorrelation matrix showing the cross-correlations between the same population ERMs to reveal positively correlated (warm colors) and anti-correlated (cool colors) areas in the population ERM. Black dashed line: choice point. (**C**) Task-congruent (TC, orange triangles) and task-incongruent (TI, blue rectangle) areas in the autocorrelation matrix (only shown in the lower half of the matrix to avoid duplicate

information). (**D** and **E**) Comparison of mean correlation coefficients between the CA1 and subiculum in the task-congruent area (D) and task-incongruent area (E). ***$p < 0.001$.

Next, I tested if the schematic representation of the subiculum could be mainly attributable to the broader firing patterns of subicular cells compared to CA1 neurons. To test it, I obtained the population ERM whose individual fields were randomly shifted and realigned (**Figure 9A**), and calculated an autocorrelation matrix based on the shifted population ERMs (**Figure 9B**) both in the CA1 and subiculum (repeated for 1000 times; see Materials and Methods for details). **Figure 9B** shows the representative autocorrelation matrices obtained for the CA1 and subiculum using the above procedures, and it is clear that the surrogate autocorrelation matrices for both CA1 and subiculum now exhibit similar, symmetric shapes of high-correlation zones along the diagonal direction (**Figure 9B**) as was observed in the CA1 when using the original population ERMs (**Figure 8B**). That is, the distinct patterns of high-correlation areas, separated by the choice point, in the autocorrelation matrix of the subiculum disappeared as the field positions were shifted. When I compared the similarity of the autocorrelation matrices between the original and shifted versions by calculating pixel-to-pixel correlations, the autocorrelation matrices composed of randomly shifted subicular ERMs were more similar to that of the CA1 than that of the subiculum ($Z = 38.72$, $p < 0.0001$, Wilcoxon rank-sum test). These results suggest that the schematic firing patterns of the subiculum may not be explained simply by the large field sizes of the subiculum.

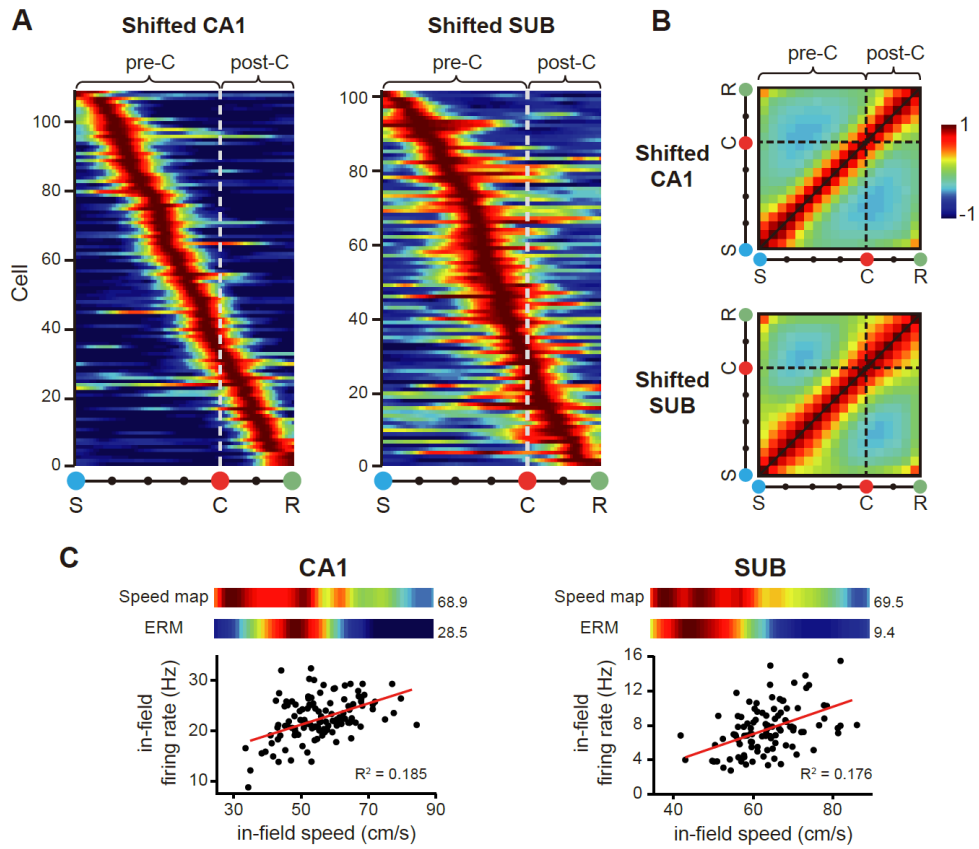

Figure 9. Large field size did not cause the schematic firing pattern of the subiculum. (**A**) Representative examples of the population ERMs containing the randomly shifted ERMs for individual cells in the CA1 and subiculum. The locations of ERMs were shuffled and sorted by their peak firing locations. Note that the characteristic schematic firing across the choice point observed in the original population ERM for the subiculum disappeared. (**B**) Averaged autocorrelation matrix using the shifted ERMs. The correlational pattern made of the shifted ERMs in the subiculum became similar to that of the CA1. (**C**) Representative examples of cells showing speed correlation in the CA1 (left) and subiculum

(right). The ERMs of the speed-correlated cells were similar to the speed maps in the corresponding session (color maps, top; numbers indicate maximal speed and firing rate), and there was a significant correlation between the in-field firing rates and their associated running speeds in individual trials (scatter plots, bottom).

Furthermore, I checked the possibility that the running speed of animal might have driven the schematic firing patterns of the subiculum described above. For this purpose, I tested whether a given cell's firing rate was significantly correlated with the animal's running speed. Specifically, I first picked the cells in which the ERM and its associated speed map were significantly correlated. Then, among those cells, I checked whether the cell's in-field firing rates for individual trials were significantly correlated with their associated running speeds (**Figure 9C**). The cells meeting these two criteria were labeled as 'speed cells' and I found some speed cells both in the CA1 (11%, n = 12/109) and subiculum (6%, n = 6/101). Importantly, excluding these cells led to the almost same results (p-values < 0.001 when comparing the correlation coefficients of the two regions in the task-congruent and task-incongruent zones). These findings suggest that the schematic neural firing patterns uniquely found in the subiculum compared to the CA1 (**Figure 10**) cannot be explained simply by the running speed of rats in the current study.

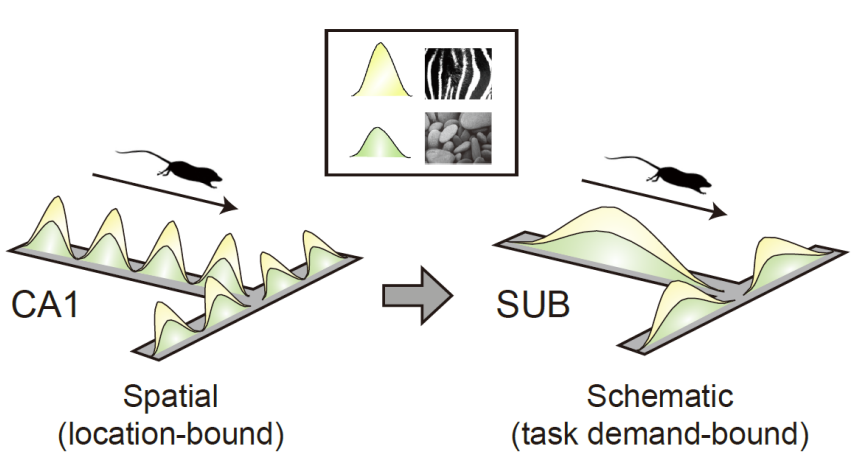

Figure 10. Illustration of the differential coding schemes between the hippocampus and subiculum. Location-specific firing patterns of CA1 cells are translated (by chunking) into schematic representations in the subiculum. Overlapping fields in different colors illustrate the scene-dependent rate remapping with each field associated with one of the visual scenes in the task.

Neurons in CA1 and subiculum were equally capable of representing visual scenes by rate modulation

I examined whether scene-based rate remapping also occurred in the subiculum when facing different visual scenes as we previously reported in the dorsal CA1 (Delcasso et al., 2014). Because no significant difference was found during analysis between the single-field and multiple-field types in the subiculum, all ERMs were used in the subiculum for analysis. Confirming our prior findings (Delcasso et al., 2014), some units in the CA1 exhibited robust rate remapping according to the rat's choice response (**Figure 11A**, cells 4-6). In contrast, other units' firing rates were modulated by visual scenes (when comparing between different scenes associated with the same choice response) (**Figure 11A**, cells 7-9). Importantly, similar rate remapping patterns were also found in the subiculum. That is, some subicular neurons changed their firing rates according to the rat's choice (**Figure 11B**, cells 13-15) and other units were more tuned to the visual scenes (**Figure 11B**, cells 16-18). In both regions, some cells were not responsive to task demands ('nonspecific units' in **Figures 11A** and **11B**).

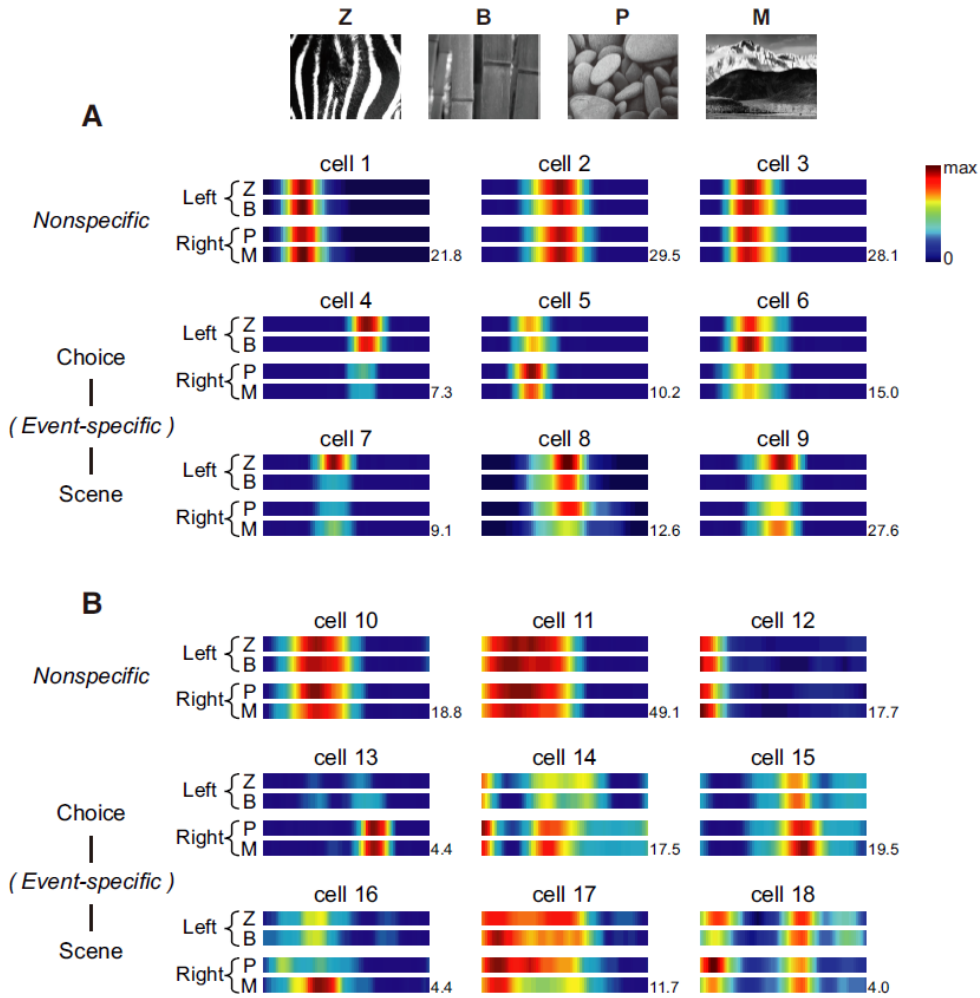

Figure 11. Task-dependent rate remapping in the CA1 and subiculum. (**A** and **B**) Representative ERMs of CA1 (A) and subicular (B) cells, associated with four scenes (Z, B, P, and M). Cells are sub-categorized into nonspecific, choice-specific and scene-specific units. Scene and associated spatial choice are labeled on the left side of each ERM. The number at the end of the ERM of each cell denotes the maximum firing rate.

To measure the amount of rate remapping, I developed a rate difference index (RDI) as follows. The RDI between the two choices (RDI_{CHOICE}) was obtained by calculating the absolute difference between the firing rate distributions associated with the left choice and right choice trial types (i.e., FR_{LEFT} or FR_{RIGHT}; **Figure 12A**). The RDI between the visual scenes within the same response type (e.g., zebra stripes and bamboo scenes for the left choice trial type; RDI_{SCN}) was obtained by calculating the difference in the firing rate distributions associated with those scenes (with the larger RDI taken between $RDI_{SCN\text{-}L}$ and $RDI_{SCN\text{-}R}$; **Figure 12B**). I found no significant difference between the CA1 and subiculum with respect to both RDI_{CHOICE} ($Z = 1.60$, $p = 0.11$, Wilcoxon rank-sum test; **Figure 13A**) and RDI_{SCN} ($Z = 0.19$, $p = 0.85$; **Figure 13B**). I also tested the possibility that the units recorded from the tetrodes located at the transition zone between the CA1 and subiculum (i.e., SUB/CA1) affected the RDI distributions. However, I found no significant difference between the CA1 and subiculum when running the same statistical tests after removing the units recorded from the SUB/CA1 (RDI_{CHOICE}: $Z = 0.41$, $p = 0.68$; RDI_{SCN}: $Z = 0.32$, $p = 0.75$; Wilcoxon rank-sum test). These findings strongly suggest that task-relevant information (i.e., scene and choice response) is represented robustly in both the CA1 and subiculum when rats perform the VSM task.

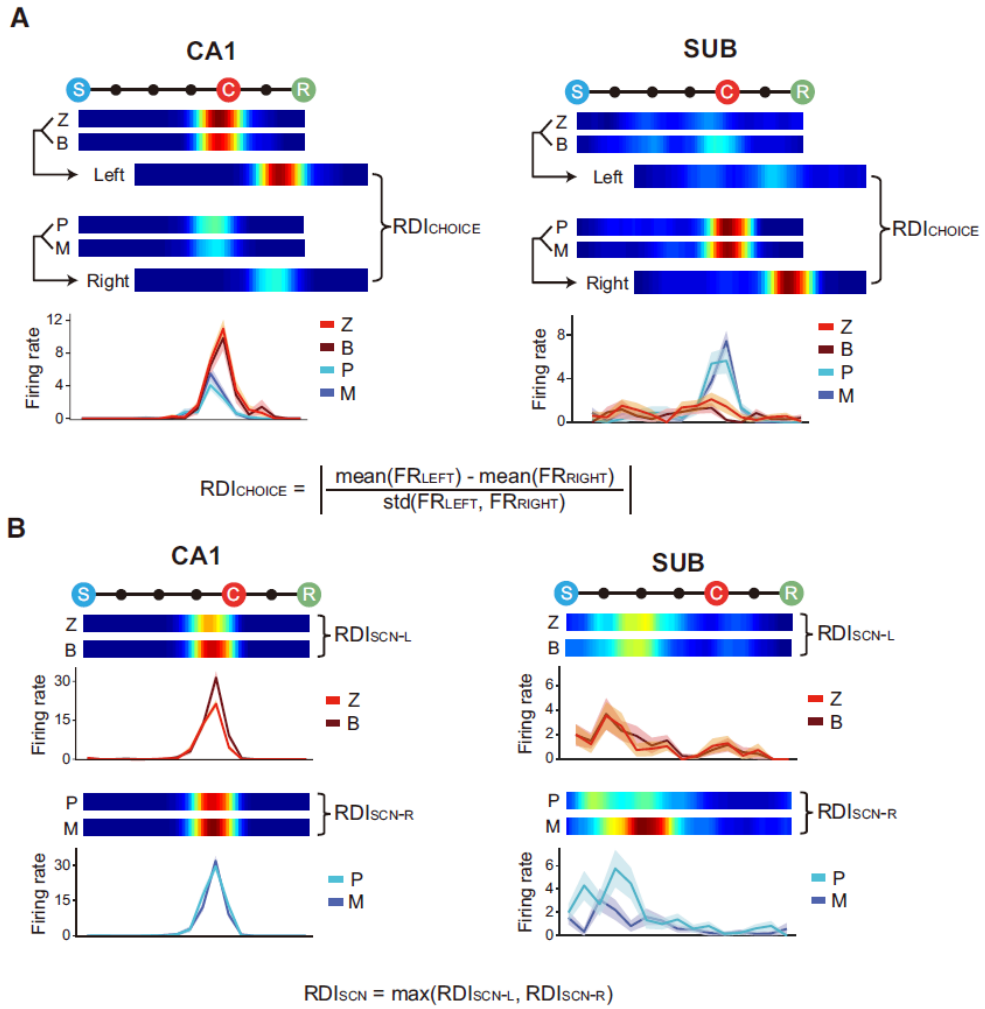

Figure 12. Calculation of rate difference index (RDI) (**A** and **B**) Illustration of the procedures for calculating the rate difference index (RDI). Each panel consists of the ERMs associated with different task-relevant information (top) and line graphs that compare the firing rates between different scene conditions along the event axis (bottom). (**A**) Rate difference index for choice (RDI_{CHOICE}). Scenes associated with the same choice arm were combined to measure the field's firing rate for each side (i.e., FR_{LEFT} and FR_{RIGHT}). RDI_{CHOICE} is the difference between the firing rates associated with the left and

right choices. (**B**) Rate difference index for the scene (RDI_{SCN}). RDI_{SCN-L} and RDI_{SCN-R} are RDI values computed for different scenes that share the common choice arm, and the larger of the two was taken as RDI_{SCN} of the cell.

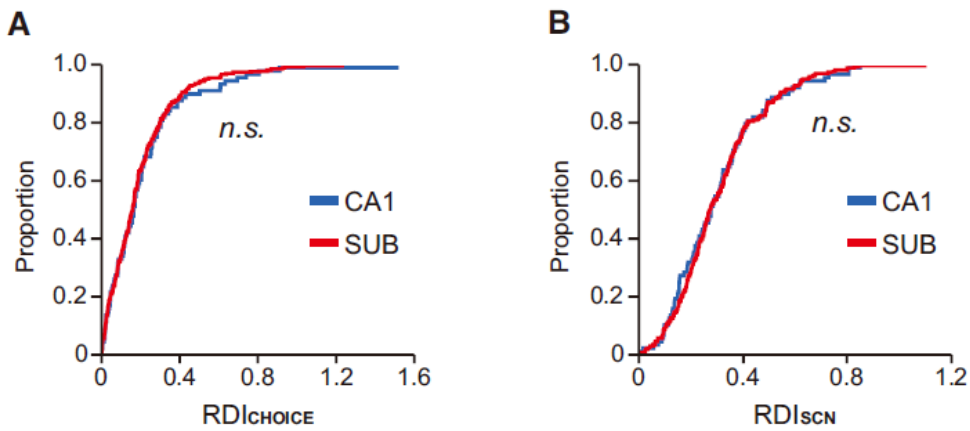

Figure 13. Comparable amount of rate remapping in the CA1 and subiculum (**A** and **B**) Cumulative distributions of RDI_{CHOICE} (A) and RDI_{SCN} (B). RDI_{CHOICE} was not significantly different between the CA1 and subiculum, and the same was the case for RDI_{SCN}.

Discussion

In the current study, I reported some differences in neural firing correlates between the CA1 and subiculum. Specifically, when examined at the population level, the neurons with single fields in the subiculum appear to cover the critical epochs of the task in a schematic (or categorical) manner, as opposed to more specific location-bound fields in the hippocampus. Despite these differences, neurons in both CA1 and subiculum showed similar amounts of rate remapping between different scenes in the visual scene memory task.

Prior studies also have reported the relatively broad fields in the subiculum (Barnes et al., 1990; Sharp and Green, 1994), but their functional significance has been unclear. The current study implies that task-related information represented by the focal fields in the CA1 may be packaged into more schematic firing fields matching the critical epochs (e.g., pre- and post-choice periods) in the subiculum. The fact that those broadly tuned cells in the subiculum conveyed scene and choice information as robustly as CA1 cells suggest that the schematic firing patterns in the subiculum may not simply stem from poor spatial firing properties. Such interpretations are also supported by the similarity within the same epoch as well as the orthogonality between different epochs in the task, both simultaneously observed in the neuronal population in the subiculum. Theoretically, it may not be necessary for an action system

downstream of the hippocampus to know where in the maze a certain scene was experienced with the greatest precision to determine its final action because a background scene is supposed to remain unchanged in a certain area in the environment. According to this scenario, the task epoch-based chunking in the subiculum might be a more practical way of processing information in the downstream regions (especially for action systems) of the hippocampus. The hippocampus may need to monitor contextual information with finer resolutions in space compared to other areas because a novel significant event may occur at any point in time and space (Knight, 1996; Vinogradova, 2001). This speculation may be connected to the phenomenon that subicular cells fired similarly when the rat experienced two adjacent chambers of different shapes (Sharp, 1997) although CA1 neurons tended to remap in those situations.

How does such a broadly tuned field arise in the subiculum when its immediate upstream structure exhibits spatially focal fields? One possibility is that efferents of multiple cells in the CA1 may converge onto a single neuron in the subiculum (O'Mara et al., 2009). If multiple afferent cells in CA1 have adjacent or partially overlapping fields, it may result in a broad single field in the receiving subicular neuron. Likewise, a subicular neuron may exhibit multiple fields if its afferent cells have non-overlapping fields. Another possibility is that the broad subicular fields may be driven largely by the upstream neocortical regions (Agster and Burwell,

2013). For example, the firing fields of neurons in the perirhinal cortex tend to cover a large segment of the environment (Bos et al., 2017). However, the range of the coverage of the perirhinal fields appears to be much broader (e.g., an entire left arm of a modified T-maze) than those observed in the subiculum in the current task. We also showed that the schematic coding could not be simply generated by large subicular fields in our task, emphasizing the importance of some structured organization of the population representations reflecting task demands. Finally, the so-called axis-tuned cells in the subiculum (Olson et al., 2017) might underlie our findings because the pre-choice and post-choice epochs in our task roughly correspond to the vertical and horizontal axes of the T-maze, respectively. However, it is unlikely that the phenomenon reported here was mainly driven by axis-tuned cells in the subiculum. This is because there were approximately 8% of cells in the subiculum that were identified as axis-tuned cells according to the previous study (Olson et al., 2017), whereas over 40% of recorded units in the subiculum showed broad single fields in our study. Also, the single-field units in the current study showed rate remapping according to the task-relevant information to the similar extent compared to CA1 cells, suggesting that the subicular cells may represent more complex task-specific components than a simple spatial component.

Place fields have been shown that represent contextual change via either rate remapping or global remapping (Colgin et al., 2008).

When the contextual change is small, the place cell tends to show rate remapping, whereas when the contextual change is large, it tends to show global remapping (Muller and Kubie, 1987; Leutgeb et al., 2005; Fyhn et al., 2007; Colgin et al., 2008). In my experiment, both CA1 and subiculum cells encoded scene information mainly by rate remapping. I found the reason for this is that the scene manipulated in the task was only a part of the entire scene experienced by the rat. The stimuli other than the presented visual scene in the monitors, such as the start box, maze wall, and surrounding environment of the maze, were way more dominant to the view of the rat. In spite of darkening the experimental room to make the visual scene in the monitors salient and increasing attention for the presented scene by training the rat to choose side according to the scene, it seems that the unchanged contextual cues affected place fields to being stable.

In addition, it is possible that the overtraining of the task reduced the involvement of hippocampus. In my experiment, rats were trained to performance criteria (over 75% correctness for each scene) before the surgery, and they were trained for the same task after the recovery until the tetrodes reached the target area. Therefore, it was often extending the training period several days for cell hunting. It has been reported that the involvement of hippocampus in the task was greatly reduced when the training lasted too long (Kim and Fanselow, 1992; Packard and McGaugh, 1996; Kitamura et al., 2017). In fact, our laboratory observed that the inactivation of either

the dorsal hippocampus or subiculum did not impair the behavioral performance in the VSM task when the training lasted for about a week after reaching the performance criteria (data has not been published). It is expected that stronger signals might appear for scene and choice information in the hippocampus if the cell activities were measured right after the task acquisition.

To my knowledge, the scene- and choice-dependent rate remapping of the subiculum in a memory task have never been reported. Together with the rate remapping previously observed in the CA1 and dorsomedial striatum in the VSM task (Delcasso et al., 2014), the subicular rate remapping reported here may support the idea that scene-dependent rate remapping is not a unique code of the hippocampus. Instead, rate remapping may be a general code used across different areas. In addition, most prior studies that recorded subiculum cell activities were conducted in a foraging paradigm (Sharp and Green, 1994; Sharp, 1997, 1999; Lever et al., 2009), which has limitations in investigating various aspects of subiculum function. In this study, I found the comparable signal of visual scene information in CA1 and subiculum, and given a paucity of subicular recording studies using mnemonic tasks (Hampson and Deadwyler, 2003), these results may add valuable information to understanding the functional significance of subicular firing patterns in a memory task.

Chapter 2. Role of the visual scene stimulus for place field formation in the CA1 and CA3

Introduction

The hippocampus proper consists of CA1, CA2, and CA3. CA1 is important because it is a final stage of hippocampal information flow where the processed information of hippocampus transmits to other brain regions (Swanson et al., 1978; Cenquizca and Swanson, 2007). Since CA3 has a unique anatomical feature, recurrent collaterals (Laurberg, 1979; Ishizuka et al., 1990), it also drew a lot of attention as CA1. Because of that, CA3 has been modeled as an autoassociative network (Mcnaughton and Morris, 1987; Treves and Rolls, 1992; Rolls, 2007; Le Duigou et al., 2014) and also suggested as a subregion that plays a key role in the hippocampal memory function. Therefore, investigating place cell activities of these two subregions is necessary to fully understand the information processing of the hippocampus.

Place cells are firing activity whenever animal runs across a specific location that called place field. Such spatial activity of place cells suggests that this principal neuron, place cell, of the hippocampus plays a key role in spatial navigation. Many research has been done to find characteristics of place cell activity, which mainly focused to find how the place field responds when the stimulus consisting of the environment changes (Muller and Kubie, 1987; Hetherington and Shapiro, 1997; Lee et al., 2004; Leutgeb et al., 2005). However, it has been rarely studied on what stimulation is

necessary for place field formation. This seems to be a result of practical limitation, that is how difficult to control the experimental environment completely. For example, if environmental stimulus gets removed one by one to find out which stimulus is important to place field formation, boundary of experimental space will still remain until the last even all the cues are gone. Then, the boundary can also be a cue to activate place field even in the simplest environment (Muller and Kubie, 1989; Quirk et al., 1990; Sharp and Green, 1994).

Therefore, I used a virtual reality (VR) system to overcome this limitation. VR has the advantage that the experimenter can freely manipulate all the components that construct the environment. In VR, it is possible to create an infinitely expandable space by removing all the boundaries, which is not possible in real environment. In addition, there is no uncontrolled odors, tactile cues nor vestibular cues that caused by movement of rat. These advantages allow experimenters to have only intended visual cue set in a testing environment.

In this chapter, I tested what can be an essential stimulus for place field formation in CA1 and CA3 using the VR system. Taking advantage of it, I constructed almost empty environment to minimize consisting components with environment to block the place field formation, and then I tried to find out which stimulus is necessary for place field formation by adding visual cues one by one in that simple environment.

Materials and methods

Subjects

Four male Long-Evans rats weighing 300–400 g were used. Water was restricted to maintain body weight at 85% of free-feeding weight, and food was available ad libitum. Animals were housed individually under a 12-h light/dark cycle. All protocols used are in compliance with the Institutional Animal Care and Use Committee of Seoul National University.

Surgery

After basic taming procedure, a hyperdrive carrying 24 tetrodes and 3 reference electrodes was implanted for recording single-unit spiking activities simultaneously from the dorsal CA1 and CA3. Other surgical procedure was same as described in Chapter 1. The target coordinates for hyperdrive implantation was -3.8 mm posterior to bregma and 3.2 mm lateral to midline. In addition to the hyperdrive, acrylic headmount structure was implanted above the skull for fixing rat's head on the virtual reality system.

Virtual reality system

The virtual reality system was designed for head-restrained rats using a game engine, Unreal Engine 4.14 (Epic Games, Inc) (**Figure 14**). The custom-made virtual environment consisted of a linear track with

visual cues aside of the track. Rats were head-restrained on the Styrofoam cylinder (diameter = 66cm, width = 20cm) to rolling it as they ran. An optical sensor positioned at the side of the cylinder measured the rotation amount of the cylinder. The sensor signal was transmitted to the Unreal Engine for controlling the actor's movement within the virtual environment. Virtual environment was presented on the three LCD monitors in front of the rat so he was forced to see the virtual environment during the experiment. Licking tube was placed right in front of the mouth of the rat so that water reward was delivered through the tube. Unreal Engine controlled the solenoid valve via Arduino to release fixed amounts of water. For each frame of the Unreal engine, a TTL signal was triggered from the Arduino to Neuralynx for the synchronization of timestamp between two systems.

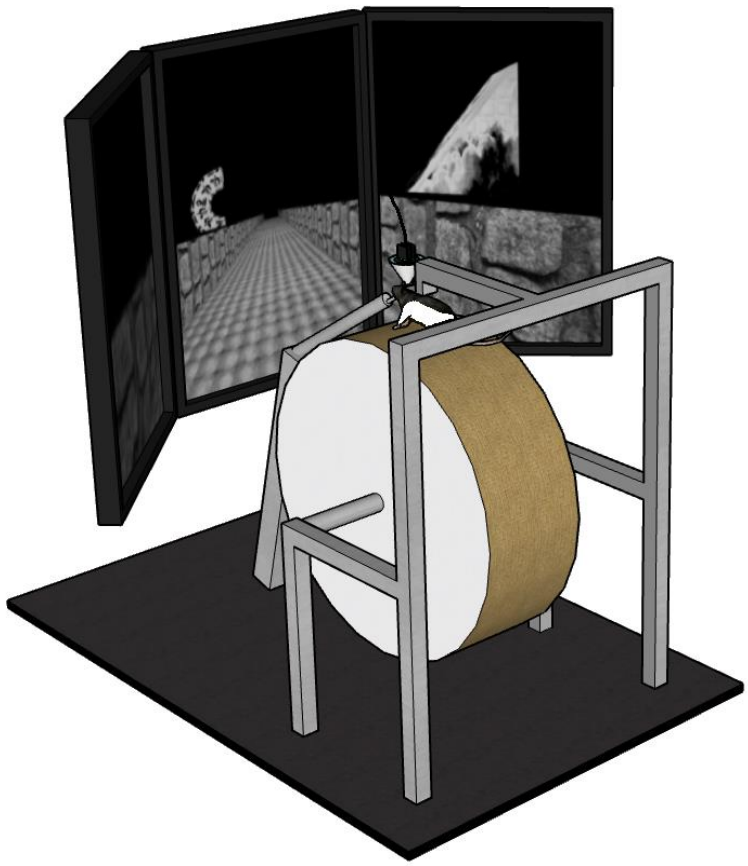

Figure 14. Virtual reality (VR) system. The virtual reality system was designed for head-restrained rats using a game engine, Unreal Engine. Virtual environment was presented on the three LCD monitors in front of the rat, and was moved as rats rolling the Styrofoam cylinder. Water reward was delivered through the tube in front of the mouth of the rat.

Virtual reality environment and recording schedule

After recovering for a week after surgery, training for running on the cylinder in the VR system was started (**Figure 15A**). Rats were restricted water, and food was available ad libitum. The VR environment for initial training was constructed with a black and white port picture (**Figure 15B**). The track is 3m long, and when the rat reaches the end of the track, it teleports to the tunnel section. The tunnel is 0.5m long and is completely dark where the surroundings are not visible except the exit at the end. When the rat reaches the end of the tunnel, it is teleported back to the start of the track. 0.25 ml of water reward was given twice for each lap within the track, not in the tunnel. The training took 30 minutes a day.

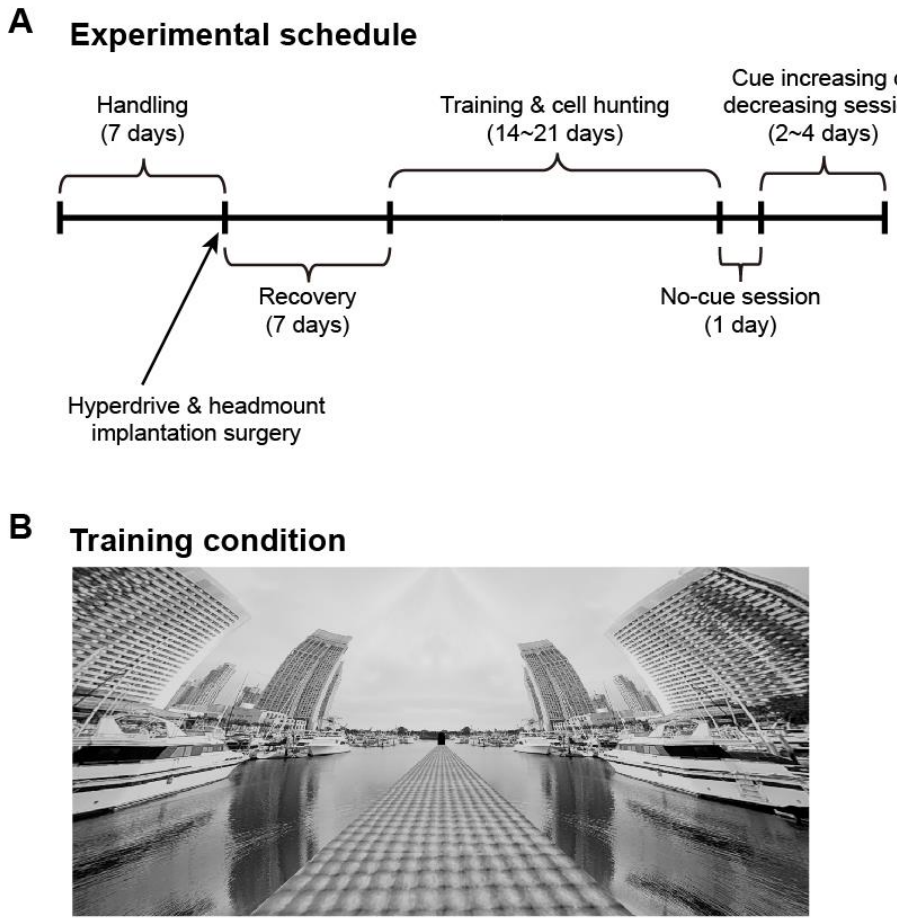

Figure 15. Experimental schedule and training environment. (A) Experimental schedule. Rats were trained to run in virtual reality system after the hyperdrive and headmount implantation surgery. During the training period, tetrodes were adjusted daily to target the CA1 and CA3 pyramidal cell layer. The recording schedule was proceeded after the training. (**B**) The rat's point of view in training condition. A black and white picture of harbor surrounded the linear track. The water rewards were given at random locations.

When the rat ran over 300m for two consecutive days for 30 minutes, the recording schedule was started. Five environments were used for recording (**Figure 16A**). First, there was No-cue condition that was made of only a 3 m long track with low walls and any other visual cues were not presented. When the rat reached the end of the track, it was teleported to the start location of the same track. Since the tunnel section was not used in between each lap, the rat continuously ran on the same track over and over. One-cue condition was made by adding a triangular cue with a black and white cloud pattern on the right side of the No-cue condition track at 165 cm. Two-cue condition was One-cue condition with second cue which was a half donut shape with a black and white Korean alphabet pattern on the left side of the track at 210 m. Three-cue condition was made by adding a cylinder shape, black and white butterfly patterned cue on the right side of the track at 255 m. Lastly, Multiple-cue condition was constructed by adding multiple cues with various shapes and colors on both sides, between the first cue and third cue of the Three-cue condition. These various cues were overlapped each other so that looked like a scene (**Figure 16B**).

On the first day of recording, rats (n = 2) ran in the No-cue session, which consisted of No-cue condition and Multiple-cue condition. In this session, rats ran on No-cue condition for 40 laps, Multiple-cue condition for 40 laps, and then No-cue condition for 40 laps again (**Figure 16C**). Other rats (n = 2) ran only on No-cue

condition for 120 trials, and these sessions were not included in the analysis. After that, the cue increasing session was conducted for 1~2 days. In the cue increasing session, conditions were given in the order of One-cue, Two-cue, Three-cue, and Multiple-cue, and each condition was presented for 30 laps (**Figure 16C**). Finally, a cue decreasing session was conducted for one day, and in this case, conditions were given in the reverse order of increasing sessions, such as Multiple-cue, Three-cue, Two-cue, and One-cue, 30 laps per each condition. For two rats, Three-cue condition was not presented, and each condition was given for 40 laps.

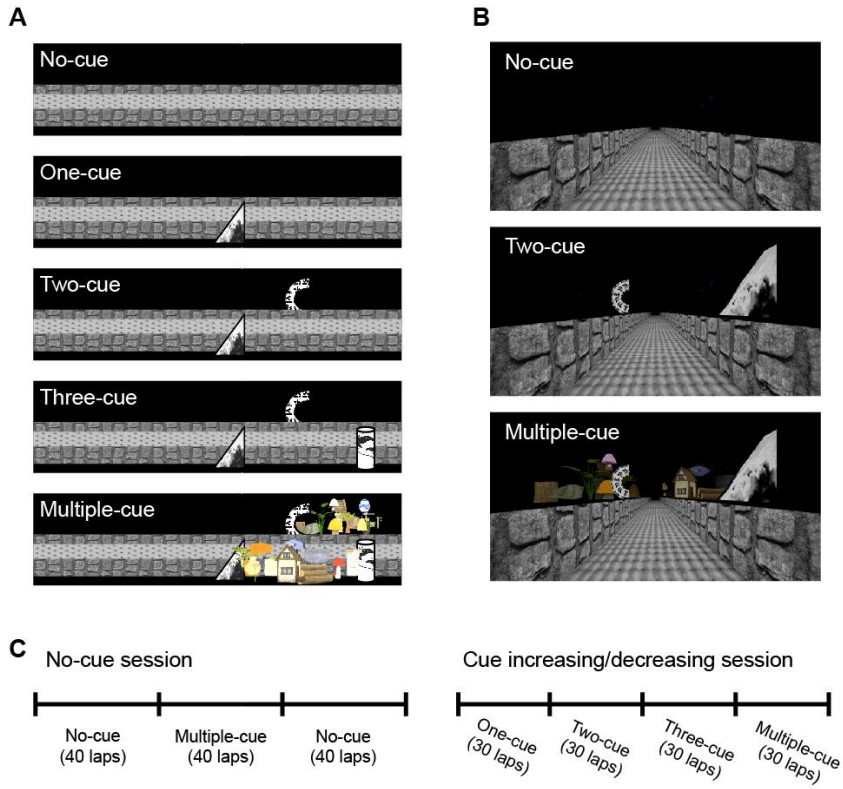

Figure 16. Virtual environment conditions and session configuration. (**A**) Diagram for experimental conditions. All conditions were constructed based on No-cue condition by adding visual cues one by one. (**B**) The rat's point of view in No-cue (top), Two-cue (middle), and Multiple-cue (bottom) conditions. In No-cue condition, there were only floor and side walls of the track. In Multiple-cue condition, visual cues were densely arranged in a scene-like fashion. (**C**) Session configurations for No-cue session (left) and Cue increasing or decreasing session (right). In No-cue session, 40-lap blocks of No-cue condition, Multiple-cue condition, and No-cue condition were sequentially presented. In cue increasing or decreasing session, 30-lap blocks of conditions were presented in ascending order or descending order, respectively.

Histology

Histology procedure was the same as described in Chapter 1. I compared the atlas (Paxinos and Watson, 2009) with Nissl stained sections to identified target region of each tetrode tip (**Figure 17**).

Unit isolation

Single units recorded in the CA1 and CA3 were isolated manually using custom-written software (WinClust) based on multiple waveform parameters, including peak and energy, as previously described (Lee and Kim, 2010; Delcasso et al., 2014; Ahn et al., 2019). Cells that had an overall mean firing rate less than 10 Hz and peak to valley width over 150 μs were classified as pyramidal neurons. Others were excluded from the analysis. Additionally, cells were filtered by their firing rate. Cells that had a mean firing rate larger than 0.5 Hz at least one condition in a session were included in further analysis.

Data analysis

Data filtering

Laps with a latency of more than 30 s were excluded because it was too long, so I assumed that the rat's running behavior was not uniform. In addition, the spike and position data of the period that was temporarily stopped, such as the rat eating the reward or taking a break, were also removed and not used for analysis.

Construction of rate map

For the construction of the rate map, the 3m long track was divided into 100 bins (bin size = 3cm). The firing rate of each bin in the raw rate map was calculated by dividing the number of spikes by the duration of occupancy for the bin. Then, the raw rate map was smoothed by using the adaptive binning method (Skaggs and McNaughton, 1993).

Significance of the spatial information score

In order to check whether the spatial information score was significantly high, the p-value for the spatial information score was calculated for each rate map. A surrogate rate map was generated by shifting the spike timestamp series forward or backward by a random amount, and spatial information score was calculated on this surrogate rate map. The process was repeated 1000 times to obtain a distribution of spatial information scores for surrogate rate maps. P-value was the ratio of surrogate spatial information score that had a higher value than the actual spatial information score.

Criteria of active cell and place cell

Cells were classified as active cells or place cells according to their rate map properties in each condition. Cells that had a mean firing rate over 0.5 Hz were classified as active cells. Cells that satisfied

the following three criteria were classified as place cells; (i) mean firing rate > 0.5 Hz, (ii) spatial information score > 0.3, (iii) p-value of spatial information score < 0.001.

Detection of place field boundaries

Detection of place field boundary was only conducted for place cells with a peak firing rate higher than 1 Hz. A place field was defined as five or more contiguous bins with firing rate over 15% of the peak firing rate of the rate map. In the VR environment, when the rat reached the end of the track, it was teleported to the start of the track. Therefore, in the field detection procedure, both ends of the track were treated as being connected. After field detection, if there was another peak showing a firing rate exceeding 50% of the peak firing rate of the map, the next field was detected in the same manner. For the second and third fields, the firing rate threshold was the same as for the first field, 15% of the peak firing rate of the map.

Categorization of remapping pattern across conditions

The remapping patterns across conditions were classified into four categories as follows. 1) Stable: a cell was classified as a place cell in both conditions, the correlation coefficient r between the two rate maps was positive, and the correlation coefficient p-value was less than 0.05; 2) Relocation: a cell was classified as a place cell in both conditions, the correlation coefficient r between the two rate maps

was either negative, or the correlation coefficient p-value was greater than 0.05; 3) No spatial activity: a cell was classified as a place cell only in one of the two conditions and was classified as an active cell in the other condition; 4) No activity: a cell was classified as a place cell in only one of the two conditions, and the mean firing rate was lower than 0.5 Hz in the other condition.

Results

Place field did not appear in the No-cue condition

I investigated which stimulus is important for the formation of the place field by taking advantage of the VR system, in which an experimenter can easily control the cues consisting of the environment. I tried to find out which stimulus effectively triggers the place field in an environment. To this end, I constructed a No-cue condition in which the place field would not be formed. In the No-cue condition, there was only the floor and the low wall of the linear track, and no other visual cue was presented. There were simple and periodic patterns on the floor and walls to provide an optic flow that allowed the rat to know movement on the track (**Figure 16B**), but there were no other cues, such as vestibular signals, tactile cues, or odor cues. Also, I made a Multiple-cue condition. In Multiple-cue condition, many visual cues were placed on both sides of the track so that the place field would be well-formed (**Figure 16**). I organized a No-cue session with 40 laps of No-cue condition, 40 laps of Multiple-cue condition, and 40 laps of No-cue condition in it so that Multiple-cue condition can be presented in between No-cue conditions (**Figure 16C**). By checking out the place field of Multiple-cue condition that inserted in between No-cue conditions, I could rule out the possibility of place field recording failure for the case when tetrode did not reach any place cell at No-cue condition.

Two rats were tested for No-cue session, where 62 of CA1 cells and 24 of CA3 cells were recorded (**Figure 17**). First, I examined the activity of recorded cells by plotting raster plots. In the Multiple-cue condition, cell firing at a specific location of the track was often observed. However, on the other hand, not a single cell showed a location-specific firing in No-cue condition (**Figure 18A**).

For quantitative verification, spatial information score was calculated for the rate map of each condition. As a result, the spatial information score of Multiple-cue condition was significantly higher than that of No-cue condition ($Z = 8.11$, $p < 0.0001$, Wilcoxon rank-sum test) (**Figure 18B**). In addition, the proportion of cells that satisfied the place cell criteria (see Materials and Methods) in Multiple-cue condition was 51.2% (39/62 = 62.9% in CA1 and n = 5/24 = 20.8% in CA3), whereas none of the cells met the place cell criteria in No-cue condition ($p < 0.0001$, Fisher's exact test).

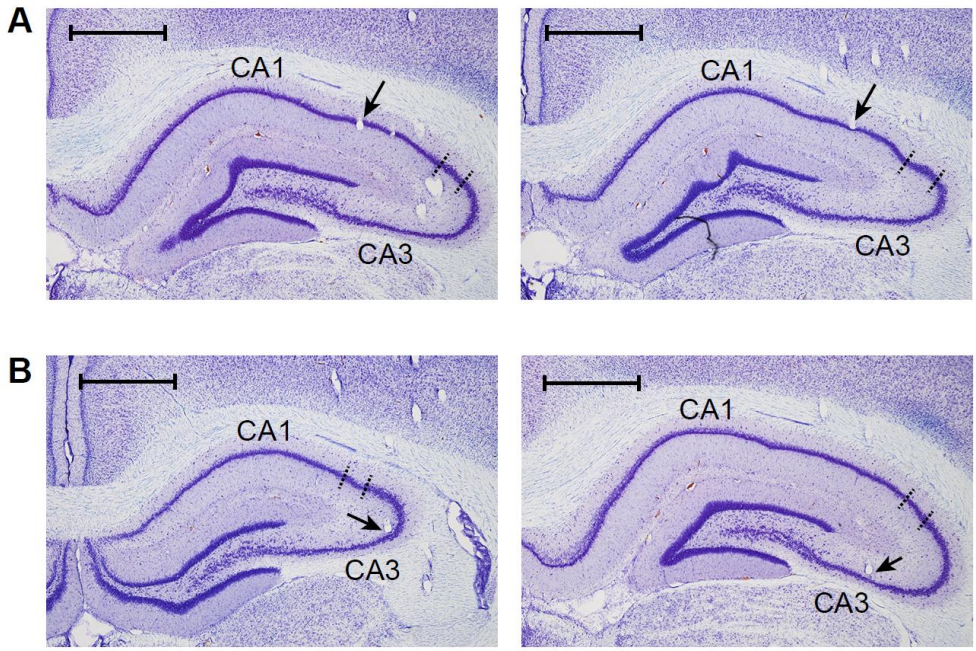

Figure 17. Simultaneous recording of single cell activities from CA1 and CA3. (**A** and **B**) Nissl-stained photomicrographs of the tissue sections showing the tetrode trajectories in (A) CA1 and (B) CA3. Dotted line denotes the boundaries between CA1, CA2, and CA3. Scale bar is 1 mm.

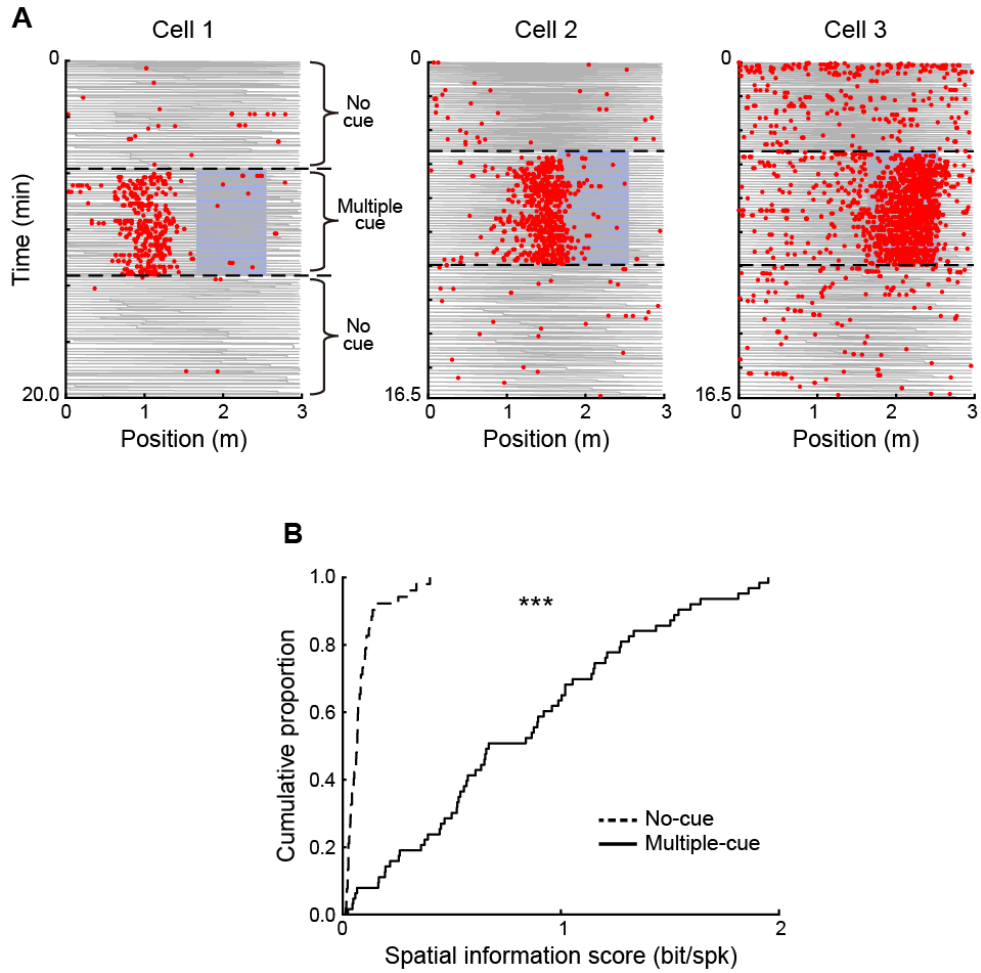

Figure 18. No spatial activity in No-cue condition. (A) Representative raster plots of cells recorded in No-cue session. Cells showed a location-specific activity in Multiple-cue condition, whereas no spatial activity was observed in No-cue condition. The Grey line represents the rat's trajectory, and the red dots are spikes. Cues were placed within the blue box. (**B**) Cumulative distribution of spatial information score. Rate maps in Multiple-cue condition had much higher spatial information score compared to those in No-cue condition. *** $p < 0.001$.

Lastly, I checked whether the spikes of No-cue condition had periodicity. If the rat formed a place field using an internal map in an environment without any cue, it is possible that the periodicity of the spike will appear with a different length than 3 meters, which is the length of the track. In order to figure this out, a spike autocorrelogram was calculated based on the location of each spike (**Figure 19B**). Cells with place fields will have a 3m periodicity length in spike autocorrelogram because they fire at a similar location on every lap, but if cells have a different length of periodicity, then that means cells might have a place field with an internal map than the actual track. Therefore, I used the fast Fourier transform (FFT) to determine which frequency showed the strongest power (**Figure 19C**). As a result, it was observed that most of the cells in Multiple-cue condition were firing every 3m, and there was no periodicity of firing cells in No-cue condition (**Figure 19D**). These results showed that there is no place field formation in No-cue condition.

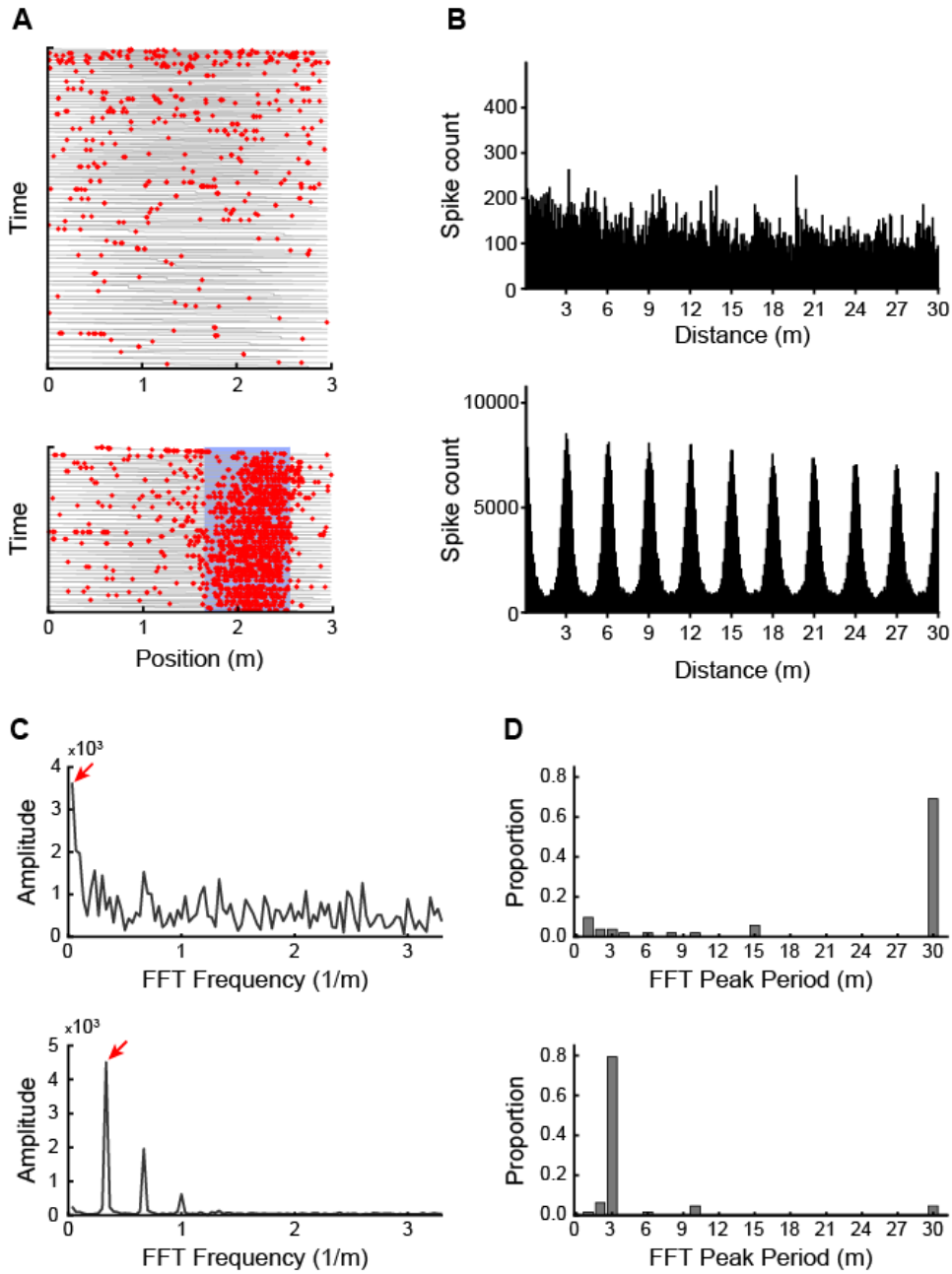

Figure 19. Fast Fourier transform (FFT) analysis results showing no periodicity in neural activity of No-cue condition. (**A**) Raster plot of an example cell. Laps were divided by their lap condition (top: No-cue condition, bottom: Multiple-cue condition). The cell had a

place field around cue locations in Multiple-cue condition. (**B**) Spike autocorrelogram graph corresponding to the cell in A (top: No-cue condition, bottom: Multiple-cue condition). The cell showed a strong periodic firing pattern with a period of 3m in Multiple-cue condition, but no periodic activity was observed in No-cue condition. (**C**) FFT results of spike autocorrelogram in B (top: No-cue condition, bottom: Multiple-cue condition). FFT successfully captured the periodicity of spike autocorrelogram in Multiple-cue condition. The inverse of peak frequency indicated by the red arrow was taken as the cell's peak period value. (**D**) Distribution of peak period for all cells (top: No-cue condition, bottom: Multiple-cue condition). Most cells in No-cue condition had a peak period value of 30 m, which is the same as the range of spike autocorrelogram. This result indicated that they did not have any periodicity at all. In multiple-cue condition, the distribution showed a dominant peak period at 3m.

Place cells responded differently to the visual cue conditions in CA1 and CA3

Next, I added visual cues to No-cue condition and observed whether a place field was formed in CA1 and CA3 (**Figure 16A**). First, One-cue condition was created to check whether a field could be formed even with a single visual cue. In addition, Two-cue and Three-cue conditions were created to check whether it is essential to have a spatial relationship between cues. Lastly, Multiple-cue condition was used to check whether it is necessary for field formation to present a scene in which many visual cues are densely arranged (**Figure 16B**). One-cue, Two-cue, and Three-cue conditions are relatively simple environments because visual cues are arranged one by one at a distance, and there are not many of them. On the other hand, in the case of Multiple-cue condition, there are many overlapped cues, and it is difficult to single out each cue, so it is a complex environment.

These conditions were presented in blocks of 30 to 40 laps each within one session and were presented in the order of increasing or decreasing the number of cues (**Figure 16C**). Four rats conducted a total of 11 sessions, and 318 of CA1 cells and 175 of CA3 cells were recorded.

In order to observe how cells respond in each condition, the firing rate map for each condition was constructed (**Figure 20**). Some CA1 cells had a place field only in one condition (cells 1~4), but there were cells having place fields in more than one condition (cells

5~8). Among those cells that had place fields in several conditions, few cells showed place fields that were maintained across conditions (cell 5). Others showed remapping when the condition changed (cells 6~8). In the case of CA3, unlike CA1, it was found that most of the cells had a field only in one condition (cells 9~12). In particular, place fields were observed frequently in Multiple-cue condition compared to other conditions (cells 11~12).

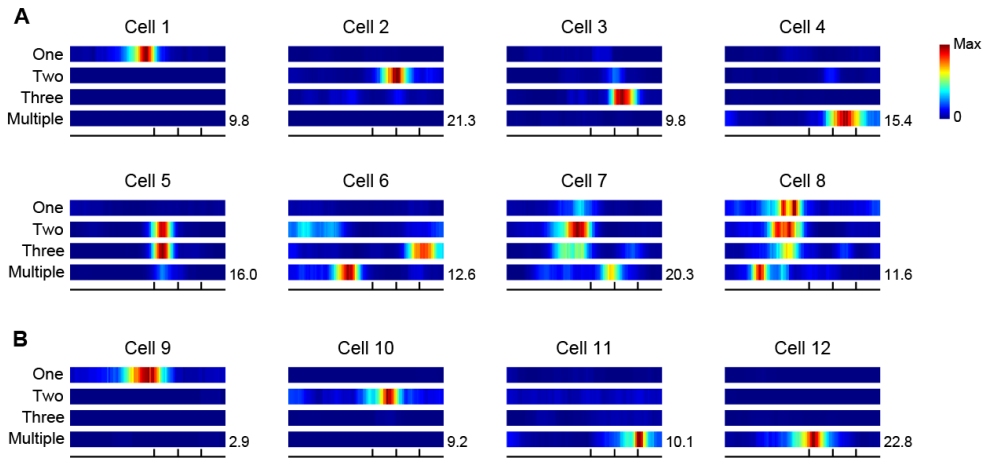

Figure 20. Representative rate maps for each cue condition. (**A**) CA1 cells were more likely to have place fields in more than one condition (cell 5~8). Place field in Cell 5 maintained its location across Two-cue and Three-cue conditions, but fields in cell 6~8 showed global remapping as the condition changed. (**B**) CA3 cells rarely had a field in multiple conditions and tended to have a field in Multiple-cue condition. The number at the right bottom side of the rate maps is a peak firing rate, and the scale bar is given on the right side. The ticks under the rate maps represent the locations of three visual cues.

I examined the activity level of hippocampal neurons according to the cue conditions. First, the proportion of active cell that had mean firing rate over 0.5 Hz was computed for each condition (**Figure 21A**). In CA1, active cell ratio was the highest in Multiple-cue condition among the four conditions, and the simple cue conditions (i.e., One-cue, Two-cue, and Three-cue conditions) showed similar proportion ($\chi^2_{(3)} = 13.5$, $p = 0.0037$, Chi-square test. Follows are post-hoc results for all condition pairs conducted by Chi-square test with Bonferroni correction. $\alpha = 0.0083$. One vs. Two-cue: $\chi^2_{(1)} = 0.24$, $p = 0.63$; One vs. Three-cue: $\chi^2_{(1)} = 1.1$, $p = 0.29$; One vs. Multiple-cue: $\chi^2_{(1)} = 7.5$, $p = 0.0063$; Two vs. Three-cue: $\chi^2_{(1)} = 2.2$, $p = 0.14$; Two vs. Multiple-cue: $\chi^2_{(1)} = 5.1$, $p = 0.025$; Three vs. Multiple-cue: $\chi^2_{(1)} = 11.7$, $p < 0.001$). CA3 also showed the highest proportion of active cell in Multiple-cue condition as well, and no statistically significant difference was observed between the simple cue conditions ($\chi^2_{(3)} = 16.6$, $p < 0.0001$, Chi-square test. Follows are post-hoc results for all condition pairs conducted by Chi-square test with Bonferroni correction. $\alpha = 0.0083$. One vs. Two-cue: $\chi^2_{(1)} = 0.2$, $p = 0.67$; One vs. Three-cue: $\chi^2_{(1)} = 6.9$, $p = 0.0085$; One vs. Multiple-cue: $\chi^2_{(1)} = 2.6$, $p = 0.11$; Two vs. Three-cue: $\chi^2_{(1)} = 5.1$, $p = 0.025$; Two vs. Multiple-cue: $\chi^2_{(1)} = 4.1$, $p = 0.042$; Three vs. Multiple-cue: $\chi^2_{(1)} = 16.4$, $p < 0.001$). Although the proportion of active cell was the highest in Multiple-cue condition in both CA1 and CA3, the

amount of difference in the proportion was only about 10%. Next, comparing mean firing rate between the conditions showed no differences between conditions in CA1 (**Figure 21B**) ($\chi^2_{(3)} = 7.5$, $p = 0.057$, Kruskal-Wallis test). In CA3, mean firing rate of Multiple-cue condition was slightly higher than that of Three-cue condition, and there was no significant difference between other condition pairs (**Figure 21B**) ($\chi^2_{(3)} = 9.79$, $p = 0.0204$, Kruskal-Wallis test. Follows are post-hoc results for all condition pairs conducted by Wilcoxon rank-sum test with Bonferroni correction. $\alpha = 0.0083$. One vs. Two-cue: $Z = 0.1$, $p = 0.91$; One vs. Three-cue: $Z = 2.2$, $p = 0.0297$; One vs. Multiple-cue: $Z = 1.1$, $p = 0.25$; Two vs. Three-cue: $Z = 2.3$, $p = 0.0192$; Two vs. Multiple-cue: $Z = 1.4$, $p = 0.16$; Three vs. Multiple-cue: $Z = 2.7$, $p = 0.0062$). Therefore, these results indicated that the visual cues did not dramatically change the overall activity level of hippocampal cells.

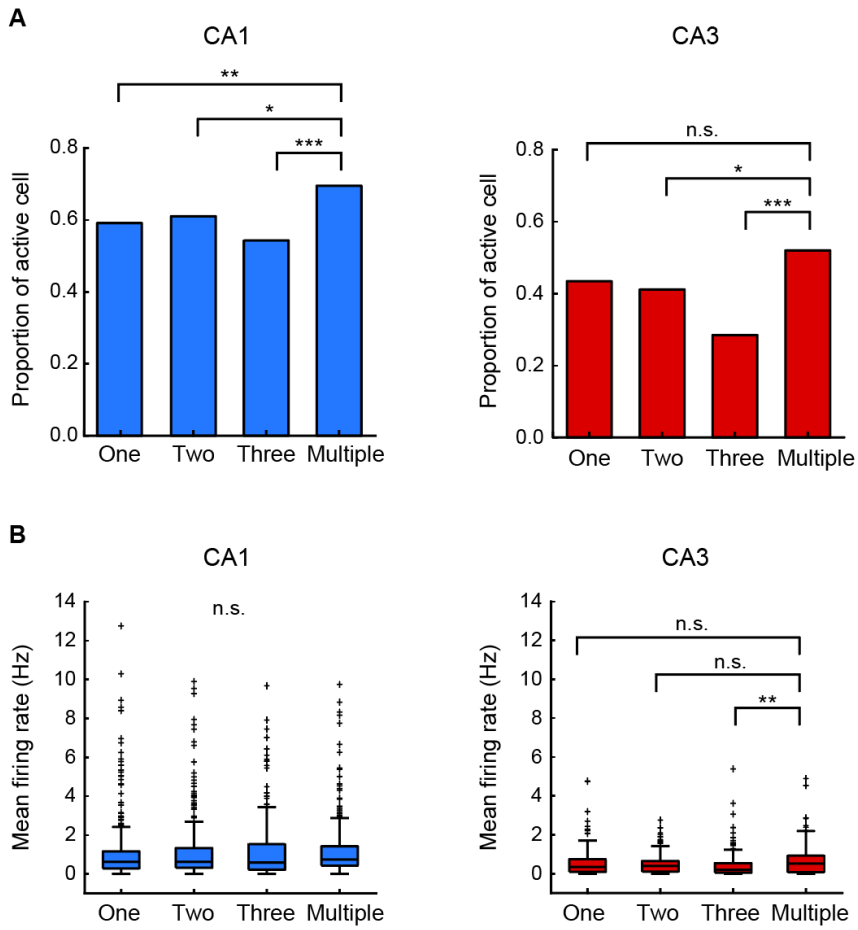

Figure 21. The number of cue had mild effect on the activity level of hippocampal cells. (**A**) Proportion of active cell for each condition. In both CA1 and CA3, active cell ratio was highest in Multiple-cue condition. No systematic change according to the number of cue was found among the simple cue conditions. (**B**) Distribution of mean firing rate for each condition. In CA1, no significant difference was observed between conditions. In CA3, mean firing rate of Multiple-cue condition was higher than that of Three-cue condition, but it was comparable with that of the other conditions. ** $p < 0.01$.

To determine how well the place field was formed in each condition, a proportion of place cells was obtained for each condition (**Figure 22**). As a result, in CA1, the proportion of place cells gradually increased as the number of cues increased, and appeared to reach asymptote at Three-cue condition ($\chi^2_{(3)} = 123.6$, $p < 0.0001$, Chi-square test. Follows are post-hoc results for all condition pairs conducted by Chi-square test with Bonferroni correction. $\alpha = 0.0083$. One vs. Two-cue: $\chi^2_{(1)} = 24.0$, $p < 0.0001$; One vs. Three-cue: $\chi^2_{(1)} = 90.2$, $p < 0.0001$; One vs. Multiple-cue: $\chi^2_{(1)} = 89.9$, $p < 0.0001$; Two vs. Three-cue: $\chi^2_{(1)} = 30.1$, $p < 0.0001$; Two vs. Multiple-cue: $\chi^2_{(1)} = 23.6$, $p < 0.0001$; Three vs. Multiple-cue: $\chi^2_{(1)} = 2.9$, $p = 0.090$). Whereas, CA3 showed no significant change in the proportion of place cells until the number of cues was increased to three, and then the place cell proportion increased as about double in Multiple-cue condition ($\chi^2_{(3)} = 14.2$, $p = 0.0026$, Chi-square test. Follows are post-hoc results for all condition pairs conducted by Chi-square test with Bonferroni correction. $\alpha = 0.0083$. One vs. Two-cue: $\chi^2_{(1)} = 0.45$, $p = 0.50$; One vs. Three-cue: $\chi^2_{(1)} = 1.09$, $p = 0.30$; One vs. Multiple-cue: $\chi^2_{(1)} = 15.40$, $p < 0.0001$; Two vs. Three-cue: $\chi^2_{(1)} = 0.22$, $p = 0.64$; Two vs. Multiple-cue: $\chi^2_{(1)} = 10.74$, $p = 0.001$; Three vs. Multiple-cue: $\chi^2_{(1)} = 4.40$, $p = 0.036$). Although the statistical comparison between the proportion of Three-cue and Multiple-cue conditions resulted only a trend, the proportion of Multiple-cue condition was

significantly higher than One and Two-cue conditions. Overall, CA3 showed a lower proportion of place cells than CA1 ($\chi^2_{(1)} = 58.06$, $p < 0.0001$, Chi-square test).

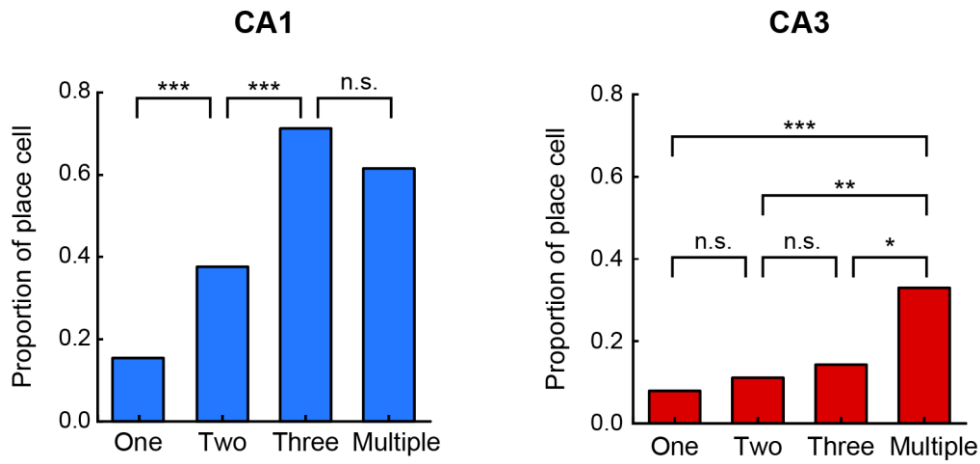

Figure 22. The proportion of place cells for each condition. The proportion of place cells gradually increased as the number of cues increased and showed a similar level in Three-cue condition and Multiple-cue condition in CA1. In CA3, no significant change in the proportion of place cells was observed until the number of cues increased to three. The proportion was only significantly increased in Multiple-cue condition. Overall, CA3 showed a lower proportion of place cells than CA1. * $p < 0.05$, *** $p < 0.001$.

I also computed spatial information score of active cells which is a continuous measurement indicating how much the rate map of each cell gives the location information of the rat, and the same trend with the place cell proportion was observed (**Figure 23A**). CA1 showed a gradual increase until the number of cues increased to three, and showed similar levels in Three-cue condition and Multiple-cue condition ($\chi^2_{(3)} = 159.91$, $p < 0.0001$, Kruskal-Wallis test. Follows are post-hoc results for all condition pairs conducted by Wilcoxon rank-sum test with Bonferroni correction. $\alpha = 0.0083$. One vs. Two-cue: $Z = 6.45$, $p < 0.0001$; One vs. Three-cue: $Z = 9.63$, $p < 0.0001$; One vs. Multiple-cue: $Z = 10.71$, $p < 0.0001$; Two vs. Three-cue: $Z = 5.67$, $p < 0.0001$; Two vs. Multiple-cue: $Z = 5.73$, $p < 0.0001$; Three vs. Multiple-cue: $Z = 0.67$, $p = 0.50$). CA3 showed a significant increase only in Multiple-cue condition ($\chi^2_{(3)} = 22.54$, $p < 0.0001$, Kruskal-Wallis test. Follows are post-hoc results for all condition pairs conducted by Wilcoxon rank-sum test with Bonferroni correction. $\alpha = 0.0083$. One vs. Two-cue: $Z = 0.77$, $p = 0.44$; One vs. Three-cue: $Z = 0.08$, $p = 0.94$; One vs. Multiple-cue: $Z = 3.98$, $p < 0.0001$; Two vs. Three-cue: $Z = 0.67$, $p = 0.50$; Two vs. Multiple-cue: $Z = 3.38$, $p = 0.0007$; Three vs. Multiple-cue: $Z = 3.46$, $p = 0.0005$), and had generally lower value compared to the CA1 ($Z = 4.05$, $p < 0.0001$, Wilcoxon rank-sum test). In addition, the same result was obtained when computing the sparsity that is a measurement indicating how much of the track is covered by the cell firing (**Figure**

23B). Sparsity of CA1 cells decreased as the number of cue increased, and Three-cue condition and Multiple-cue condition had comparable values ($\chi^2_{(3)} = 157.28$, $p < 0.0001$, Kruskal-Wallis test. Follows are post-hoc results for all condition pairs conducted by Wilcoxon rank-sum test with Bonferroni correction. $\alpha = 0.0083$. One vs. Two-cue: $Z = 6.26$, $p < 0.0001$; One vs. Three-cue: $Z = 9.60$, $p < 0.0001$; One vs. Multiple-cue: $Z = 10.67$, $p < 0.0001$; Two vs. Three-cue: $Z = 5.64$, $p < 0.0001$; Two vs. Multiple-cue: $Z = 5.61$, $p < 0.0001$; Three vs. Multiple-cue: $Z = 0.88$, $p = 0.38$). In CA3, sparsity was significantly low only for Multiple-cue condition ($\chi^2_{(3)} = 23.36$, $p < 0.0001$, Kruskal-Wallis test. Follows are post-hoc results for all condition pairs conducted by Wilcoxon rank-sum test with Bonferroni correction. $\alpha = 0.0083$. One vs. Two-cue: $Z = 0.86$, $p = 0.39$; One vs. Three-cue: $Z = 0.16$, $p = 0.88$; One vs. Multiple-cue: $Z = 4.15$, $p < 0.0001$; Two vs. Three-cue: $Z = 0.71$, $p = 0.48$; Two vs. Multiple-cue: $Z = 3.28$, $p = 0.0011$; Three vs. Multiple-cue: $Z = 3.56$, $p = 0.0004$).

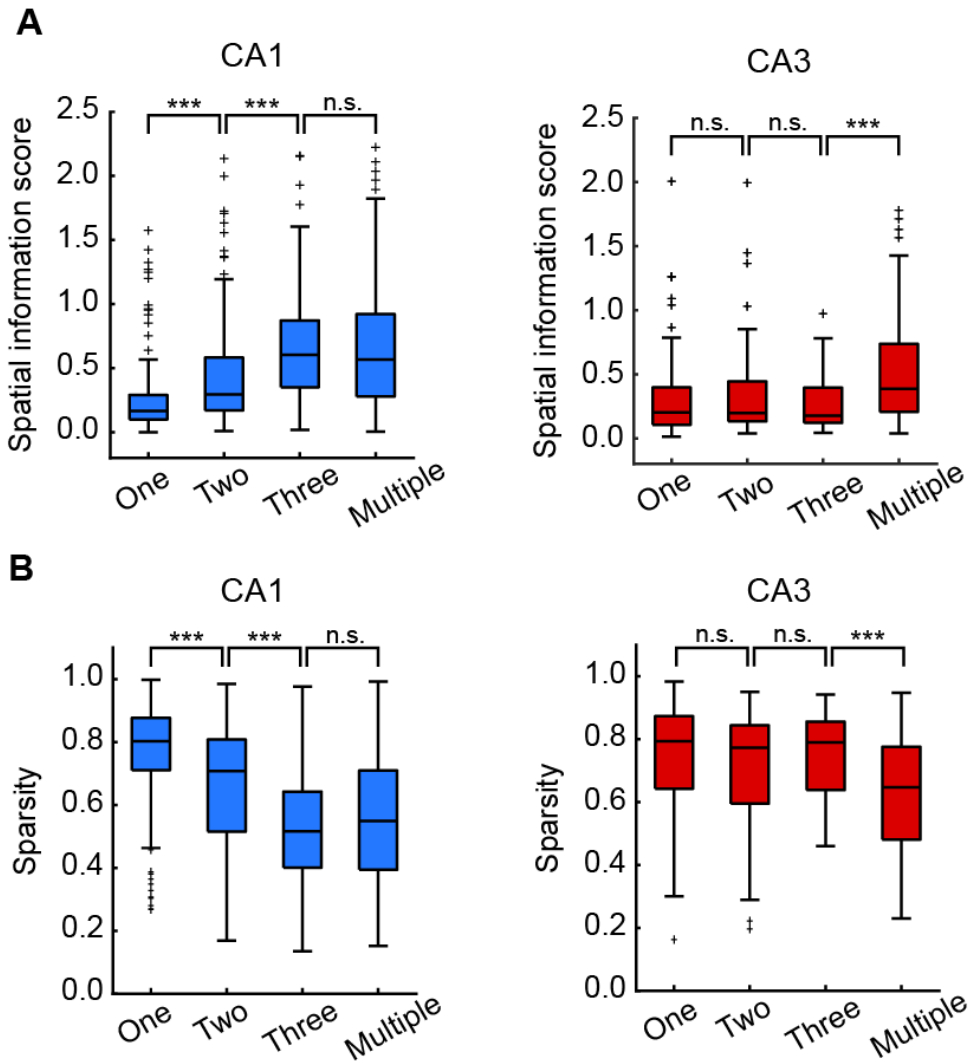

Figure 23. Distribution of spatial information score and sparsity showing the same trend as in the place cell proportion. Box plots showed the distribution of (**A**) spatial information score and (**B**) sparsity for each condition in CA1 and CA3. (**A**) CA1 showed a gradual increase in spatial information score until the number of cues increased to three and showed similar levels in Three-cue condition and Multiple-cue condition. CA3 showed a significant increase in spatial information score only in Multiple-cue condition and

generally had a lower value compared to the CA1. (**B**) The sparsity of CA1 decreased as the number of cue increased. Only the pair of Three-cue and Multiple-cue had comparable sparsity value. In CA3, the distribution of sparsity in Multiple-cue was significantly smaller than other conditions. *** $p < 0.001$.

To exclude the possibility that the order of conditions caused the activity change of hippocampal cells, I conducted two types of sessions with different condition sequences. In one type of session, conditions were presented in increasing order of cue (i.e., one-two-three-multiple), and in the other, conditions were presented in decreasing order of cue (i.e., multiple-three-two-one). Then, the proportion of place cells was computed separately for each session type. Although the trend of CA3 was not identified because the number of CA3 cells recorded in the session of decreasing number of cue was insufficient, CA1 cells showed similar pattern in both session types (**Figure 24**). As the number of cue increased, the proportion of place cell gradually increased, and reached asymptote at Three-cue condition in both the cue increasing session ($\chi^2_{(3)} = 79.4$, $p < 0.0001$, Chi-square test. Follows are post-hoc results for adjacent condition pairs conducted by Chi-square test with Bonferroni correction. $\alpha = 0.0167$. One vs. Two-cue: $\chi^2_{(1)} = 19.2$, $p < 0.0001$; Two vs. Three-cue: $\chi^2_{(1)} = 17.1$, $p < 0.0001$; Three vs. Multiple-cue: $\chi^2_{(1)} = 2.4$, $p = 0.12$) and the cue decreasing session ($\chi^2_{(3)} = 43.1$, $p < 0.0001$, Chi-square test. Follows are post-hoc results for adjacent condition pairs conducted by Chi-square test with Bonferroni correction. $\alpha = 0.0167$. One vs. Two-cue: $\chi^2_{(1)} = 5.0$, $p = 0.025$; Two vs. Three-cue: $\chi^2_{(1)} = 12.9$, $p = 0.0003$; Three vs. Multiple-cue: $\chi^2_{(1)} = 0.4$, $p = 0.54$). Since the trend of proportion of place cells were similar in these two types of session, it seems that the effect of

condition sequence to the place field formation was negligible.

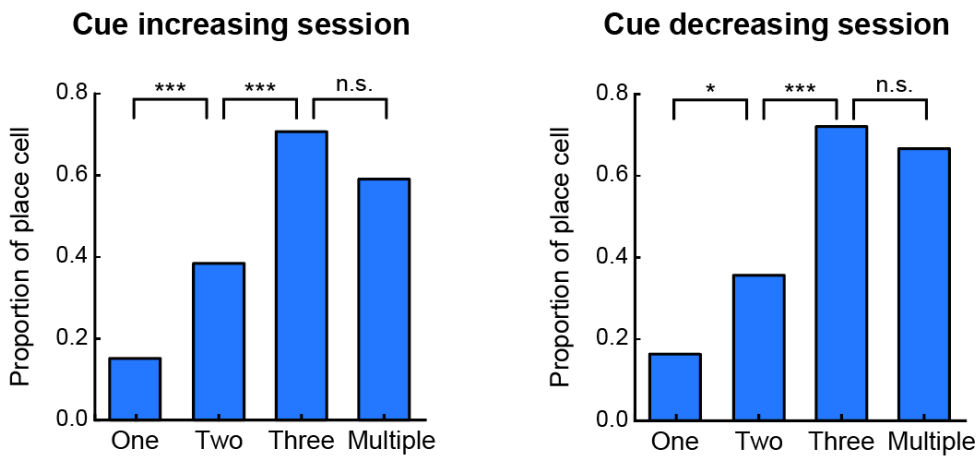

Figure 24. The order of condition did not affect the proportion of place cells. The proportion of place cells in the CA1 was computed separately for two session types. In one session type, the conditions were presented in ascending number of cue, and in the other, the conditions were presented in descending number of cue. The trend of place cell ratio was similar in two session types, which indicated that the order of conditions had little influence to the place field formation. * $p < 0.05$, *** $p < 0.001$.

To examine the distribution of place fields, I sorted the rate maps of CA1 based on their peak positions (**Figure 25**). Consistent with the prior study (Bourboulou et al., 2019), place fields were mainly distributed near the visual cues. In One-cue condition, it was observed that a large number of fields were concentrated just before the cue, and as the number of cues increased to two or three, the number of place fields encoding the location near the cue was increased together. Therefore, it was confirmed that place fields were not generated at random locations on the track but were mainly formed in a space near the cue where the rat can use the visual cues as a reference.

Based on these results, it seems that the number of place fields in CA1 increased as the space defined by the cues expanded. Whereas, cells in CA3 hardly responded to individual cues (i.e., simple cue conditions) even if the number of cues was increased to three. CA3 cells seem to be involved only when processing a lot of cues at a time (i.e., complex cue condition).

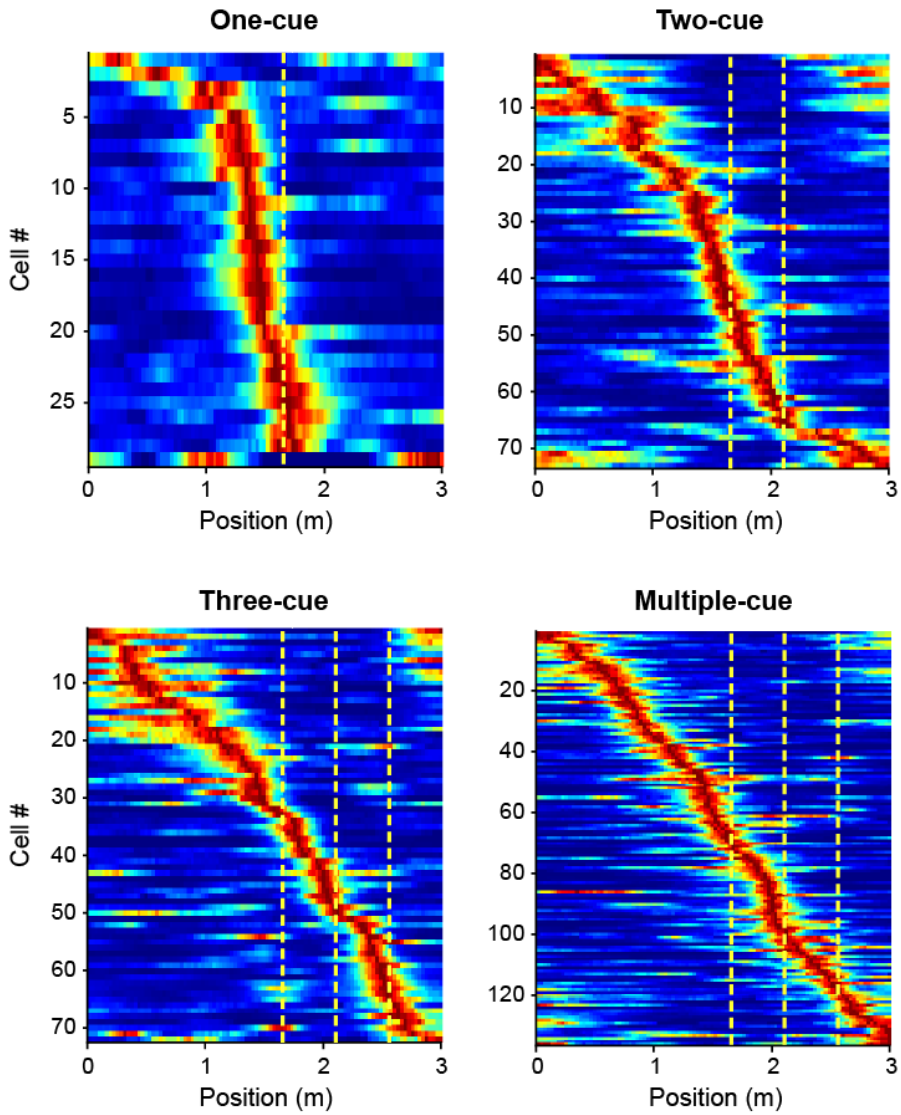

Figure 25. Place cells tended to have fields near the cue location. Rate maps of place cells were sorted according to their peak location for each condition. Most place fields were found at right before the visual cue in One-cue condition. As the number of cues increased, the distribution of place fields was spread, but the high density of place fields near the cue location was observed in all conditions. The Yellow dashed line represents the location of visual cues.

Representation of the environment in CA3 was highly orthogonal

As mentioned above, unlike CA1, most CA3 cells had a place field only in one condition, so that the field disappeared when the condition changed (**Figure 20**). I quantified how the cell activity changed between adjacent condition pairs. Activity patterns for a pair of conditions were classified into the following four categories: 1) Stable: when both conditions had a place field and the location of fields were the same; 2) Relocation: when both conditions had a place field, but the location of fields was different; 3) No spatial activity: when only one condition had a place field and the firing rate in another condition was larger than 0.5 Hz; 4) No activity: when only one condition had a place field and the firing rate in another condition was less than 0.5 Hz.

In this classification, it was observed that CA1 maintained a stable field ratio of about 20-40% (**Figure 26**). In particular, in the Two vs. Three-cue condition, the proportion of stable fields was about 40%, which was twice as high as the other condition pairs. This difference of proportion was thought to be related to the degree of change in the environment. In the case of the One vs. Two-cue condition, the number of cues doubled, and in the Three vs. Multiple-cue condition, more than ten cues were added, so there was a substantial change. However, in the case of Two vs. Three-cue condition, the number of cues increased from 2 to 3, which is 1.5 times increase, so it can be said that the degree of change in the

environment was relatively small. In the case of CA3, a stable field was hardly found, and most of the place cells were classified as No activity, showing the CA3 cells usually became silent when the environment changed (**Figure 26**). This remapping pattern of CA3 was significantly different that of CA1 (One vs. Two-cue pair: $p < 0.001$; Two vs. Three-cue pair: $p = 0.002$; Three vs. Multiple-cue pair: $p = 0.009$, Freeman-Halton exact test).

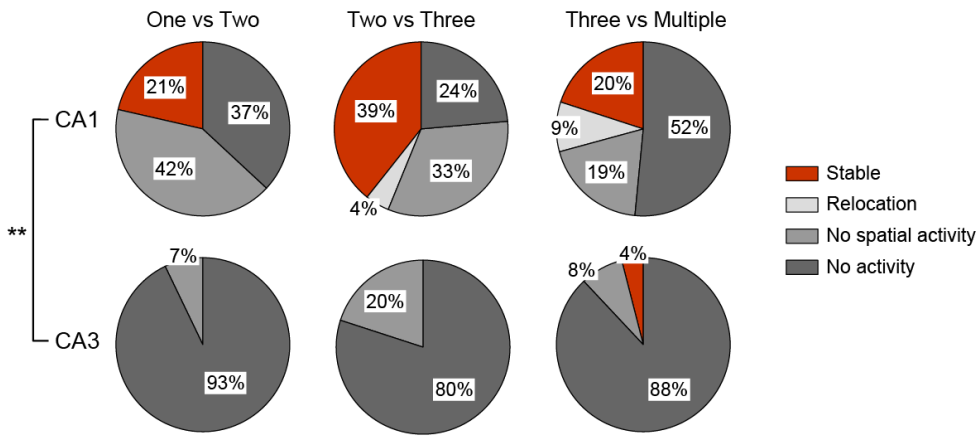

Figure 26. CA1 had a bigger proportion of stable fields than CA3. The rate maps for adjacent condition pairs were classified into four categories according to their activity pattern, which was stable, relocation, no spatial activity, and no activity. CA1 and CA3 showed significantly different proportions, where the CA1 had a larger proportion of Stable field, and cells in CA3 were mostly categorized as No activity. ** $p < 0.01$.

In addition, I counted how many conditions each cell had a place field (**Figure 27A**). Although most CA1 cells had fields in only one condition, about 30% of cells had place fields in two or more conditions. Whereas, about 90% of CA3 cells had place fields in one condition, indicating that they had fields only in a limited number of conditions compared to CA1 ($Z = 3.47$, $p = 0.0005$, Wilcoxon rank-sum test). Regardless of the place field, I also counted the number of conditions in which each cell showed activity (i.e., mean firing rate over 0.5 Hz; **Figure 27B**). Again, it was found that the CA3 cells fired in significantly fewer conditions compared to the CA1 cells ($Z = 4.79$, $p < 0.0001$, Wilcoxon rank-sum test). These results showed that the CA3 cells had a completely different representation for each condition and showed higher orthogonality than CA1 cells.

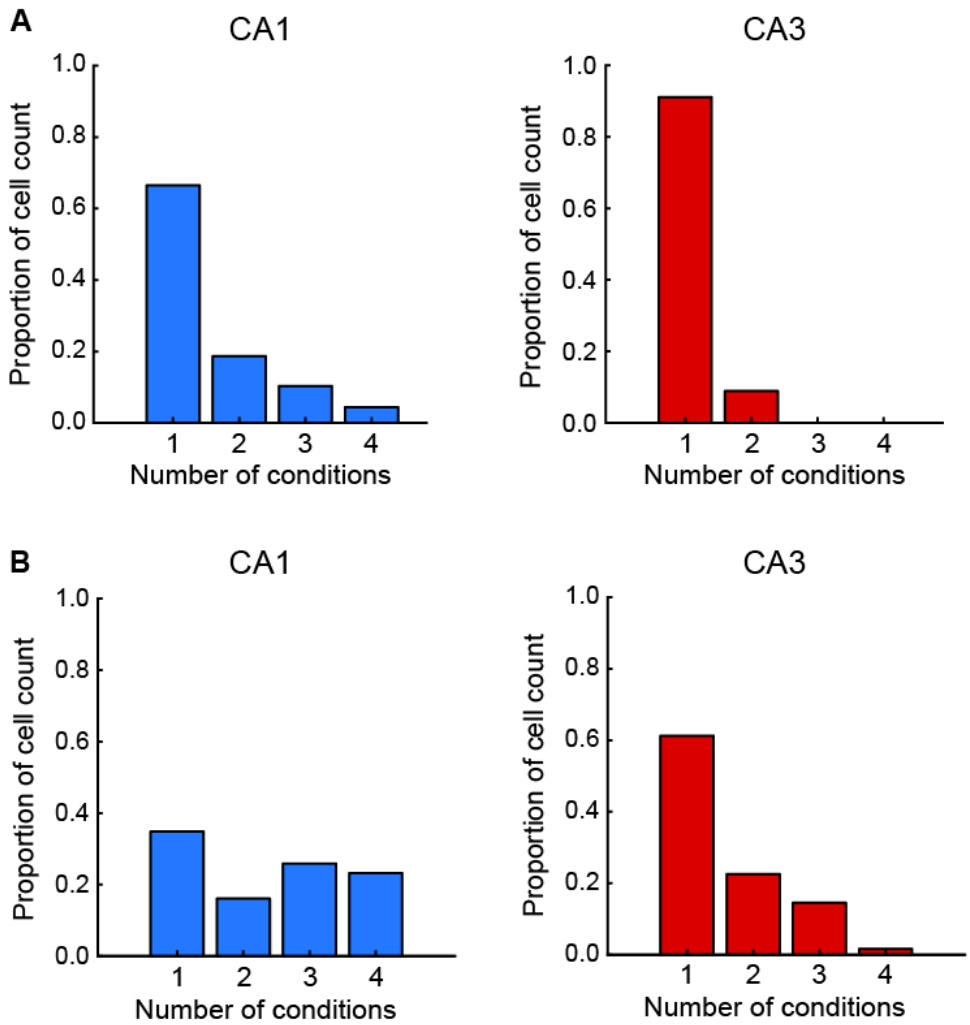

Figure 27. Most CA3 cells had a place field in one condition exclusively. The number of conditions in which the cell had place fields (**A**) or was active (**B**). CA3 cells had place fields in a smaller number of conditions compared to the CA1 cells. It was rare to observe that CA3 cells had place fields in more than one condition. The number of conditions in which the cells were active was smaller in CA3 than CA1.

Discussion

In the current study, I used the advantage of VR, in which an experimenter could completely control the cue consisting of the environment, to construct a condition where no place field was formed. Based on this condition, I investigated which visual stimulus was important for the formation of place fields in CA1 and CA3. In the case of CA1, it was observed that the ratio of place cells increased as the number of individual cues arranged in the environment increased, indicating that CA1 cells respond to simple cues and encode the space defined by the cues. On the other hand, in CA3, the ratio of place cells remained remarkably low even when the number of cues increased to three. Place cell ratio increased only for the condition where multiple cues were densely arranged, indicating that CA3 cells form a place field in response to a complex stimulus that looks like a scene. In other words, CA3 cells did not participate in the processing of simple cues and only involved in representing a complex situation. In addition, CA1 cells often showed place fields across several conditions, and about 20% of cells were found to maintain the field even when the number of cues changed. Whereas, most CA3 cells had a field only in one condition and showed no activity in other conditions, indicating a higher orthogonal coding pattern in CA3.

I considered a plausible mechanism that could explain the

difference between CA1 and CA3 in responding to the simple and complex visual cues. CA3 is anatomically characterized by a large number of recurrent collaterals (Laurberg, 1979; Ishizuka et al., 1990), and it has been modeled as an autoassociative network due to its recurrent collaterals (Mcnaughton and Morris, 1987; Treves and Rolls, 1992; Rolls, 2007; Le Duigou et al., 2014). Recurrent collateral is a key structure that allows CA3 pyramidal cells to alter their synaptic efficacy depending on the pre and postsynaptic neurons' activity (Debanne et al., 1998; Bains et al., 1999), and that enables the representation of CA3 to be reinforced and well maintained. However, this recurrent collateral does not connect all pairs of CA3 cells. It is known that one CA3 cell receives about 12,000 recurrent collateral synapses (Amaral et al., 1990; Treves and Rolls, 1992), and considering that the number of CA3 cells is about 330,000 (Amaral et al., 1990; Treves and Rolls, 1992), and one cell receives input through the recurrent collateral only from 3.6% of total CA3 pyramidal cells. Therefore, since there are quite a lot of CA3 cell pairs that are not directly connected each other, the probability of both pre and postsynaptic cells of recurrent collateral being active is not that high. So, if a sufficient number of CA3 cells are not active within the time window in which the synaptic plasticity can occur, then only few recurrent collaterals change their efficacy because active cell pairs would be rare.

For example, as shown in the figure (**Figure 28**), suppose

there are twelve hypothetical cells, and each cell is sending collaterals to four different cells (grey arrows). When a strong input comes into this hypothetical network (**Figure 28A**), five cells (cell 3, 4, 7, 9, and 12) are firing. Then, the activities are transmitted through the axons of these five cells (black arrows), and in the case of both pre and postsynaptic neurons firing (red arrows), the synapse will be strengthened so that the firing can occur easily. In addition, for the cell 7, 9 and 12, they have projections to each other (bold red arrows), which allows their activity to be maintained and strengthened for a longer time through reverberate activity (Hebb, 1964). Therefore, when a sufficient number of cells are active, they can show strong activity by utilizing the recurrent collateral. On the other hand, when a weak input enters the hypothetical network, only a small number of cells become active (**Figure 28B**). As a response to the input, two cells (cells 3 and 12) are firing, and the corresponding axons transmit the activity (black arrows). In this case, the recurrent collateral is not strengthened because there is no active cell among the postsynaptic neurons, and the activity of the network is easily extinguished. As such, CA3 networks may be able to take advantage of recurrent collaterals only when sufficient input comes into the network and activates an ensemble of CA3 cells larger than a certain threshold level within the time window where synaptic plasticity occurs in CA3.

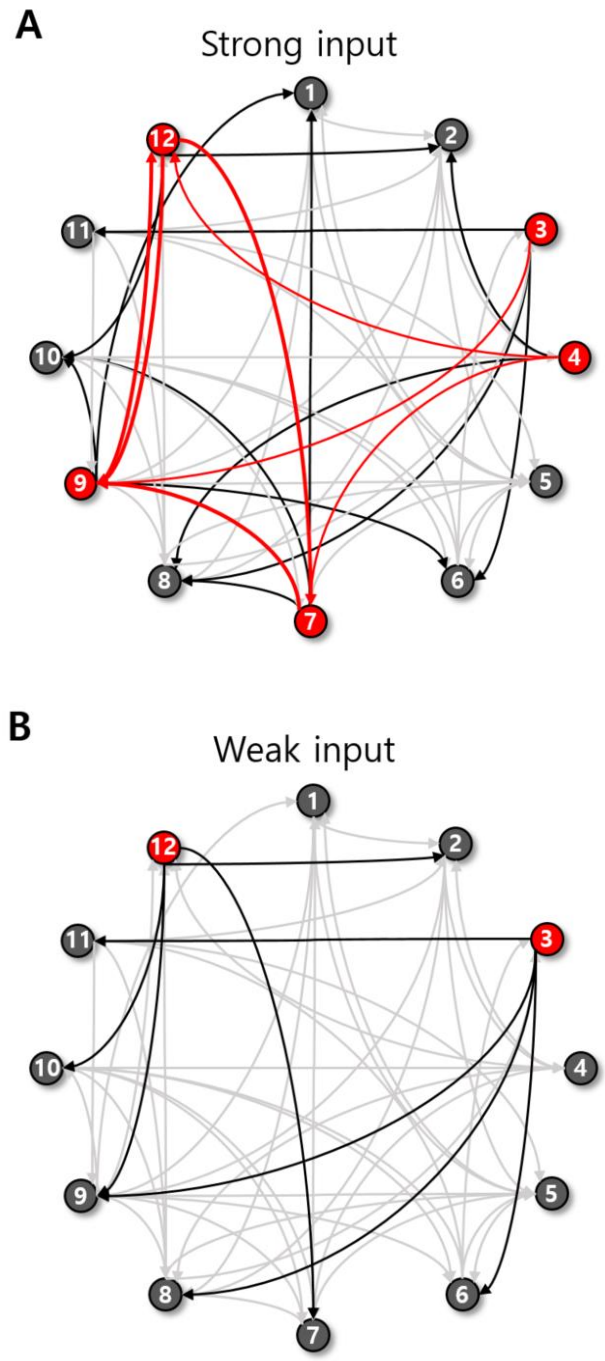

Figure 28. A hypothetical network with recurrent collaterals predicted the extinction of weak input. (**A**) Twelve cells with four recurrent collaterals consisted of a hypothetical network. A strong

input enters into this network and activates five cells (cells 3, 4, 7, 9, and 12 are denoted as red color). The activities are transmitted through corresponding axons (black arrows). For those axons of which both pre and postsynaptic neurons are firing, the synaptic efficacy is enhanced (red arrows). Especially, cells 7, 9, and 12 form a closed circuit in which the activity of this circuit could be reverberating (bold red arrows). (**B**) When a weak input comes into the network, only two cells become active (cells 3 and 12 in red color). In this case, since the active axons (black arrows) have no active postsynaptic neurons, there is no synaptic enhancement. Therefore, sufficient input is required to utilize the recurrent collateral for enhancing and maintaining the activity in the network.

To apply the suggesting model to the CA3 network, it needs to be confirm that CA3 received strong input and large number of cells were active in Multiple-cue condition. However, the active cell ratio and mean firing rate did not dramatically increase in response to the increasing number of cue (**Figure 21**), which indicated that the increasing number of cue did not enhance the extent of input. Instead, it seems that the cue aligns the input entering the hippocampal networks. In fact, it has been reported that cells in the entorhinal cortex responded to the location of objects (Deshmukh and Knierim, 2011; Tsao et al., 2013; Wang et al., 2018; Hoydal et al., 2019). Therefore, these inputs aligned to the cues would contribute the formation of place field so the proportion of place cell was high in Multiple-cue condition. The suggesting model requires a large group of co-firing cells to settle a new representation in the network by adjusting the synaptic efficacy. The activity of place cell is well fitted to this requirement because place cells show co-firing regularly with other place cells who have overlapped place fields. Whereas, the active cells without place fields show random and irregular activity so it would be difficult to adjust synaptic efficacy with the activity of active cell population. Therefore, a sufficient number of place cell might be needed to the CA3 network for establish a stable representation.

In addition, active inhibition by recurrent collaterals may contribute to different responses of CA3 to simple cues and complex

cues. The memories of previous experiences would be stored as changes in synaptic efficacy of the recurrent collaterals, and when a new input enters to CA3, it does not match the stored representation. The new representation then could be inhibited by recurrent collaterals. In fact, the active inhibition induced by recurrent collaterals has been suggested in the model of Treves and Rolls (1992), and it has been reported that the long term depression (LTD) occurs as well as long term potentiation (LTP) in the synapse of the recurrent collaterals (Debanne et al., 1998). Therefore, weak inputs entering the CA3 may not be properly settled in the network and washed out due to this active inhibition induced by recurrent collaterals.

If it works like the above-mentioned mechanism, it is thought that the amount of incoming input per unit time would be a critical factor in determining whether CA3 responds to the input. So, even if the number of cues is much larger than three, it is expected that CA3 cells are not going to respond if those cues are located apart. Also, in this experiment, only visual cues were tested because of their ease of control, but I thought that similar results would appear for other modality. For example, for the case of auditory stimulus, the amount of input would be different between a simple tone and symphony sound. Therefore, it is expected that the CA3 responds only to the latter stimulus.

On the other hand, since CA1 does not have such recurrent

collateral, it is considered to represent the incoming input without reduction or magnification. It has been reported that the CA3 showed a non-linear response to the input, but CA1 shows a linear response in both rodent studies (Guzowski et al., 2004; Lee et al., 2004; Leutgeb et al., 2004; Vazdarjanova and Guzowski, 2004) and human study (Lacy et al., 2011). In the current study, for the simple cue conditions, CA3 only showed scarce activity, so there would be less input went to CA1 through the Schaffer collateral. Then, the CA1 was more likely to represent the external sensory stimuli because it was affected by EC rather than CA3 (Lee et al., 2004). Considering that the place field of CA1 is able to be developed solely by the EC input when CA3 is lesioned (Brun et al., 2002), it seems that the place field of the CA1 in the simple cue conditions largely relied on the information from EC.

In the current study, the representation of CA3 for each condition was highly orthogonal. This result is consistent with previous studies in which the CA3 showed high orthogonality of the representation by pattern separation (Leutgeb et al., 2004; Vazdarjanova and Guzowski, 2004; Leutgeb et al., 2007). This orthogonal coding is essential for CA3 to reduce memory interference in autoassociative networks (Skaggs and McNaughton, 1992). In addition, sparsity is also required to maximize the memory capacity while maintaining the orthogonality (Skaggs and McNaughton, 1992; Alme et al., 2014), and I also observed sparse coding of CA3. Place

cell proportion and their activity level were generally low in the CA3 compared to the CA1, even in Multiple-cue condition. This low ratio of place cells in the CA3 was also observed in other cue enriched VR environments of our laboratory (not published) and in the real environment (Mizuseki et al., 2012). In an immediate early gene study, the transcription level of Arc and H1a showing the activity history of hippocampal neurons, was twice higher in CA1 than CA3 (Vazdarjanova and Guzowski, 2004) when rats foraged an open chamber.

To my knowledge, this is the first experiment creating an environment where the place field does not appear. Previously, there was a similar experiment in which the place cell was recorded during head-restrained mice running on a linear belt without any cue (Villette et al., 2015). In that experiment, the activity of CA1 cells appeared sequentially. However, in my experiment, I could not observe any regular neural activity in the hippocampus when there was no cue at all. One possible reason for this difference might be a small ensemble size recorded in the current experiment. Villette and colleagues acquired activities from hundreds neurons in a session by calcium imaging, and only 5% of them showed sequential activity. This proportion is quite small so it might not be able to capture this regular cell activity with small ensemble size recorded by hyperdrive in the current study. Another possible reason for this discrepancy of the results may be a differences in behavior paradigm. In the

experiment of Villette and colleagues, the mouse was not deprived of water and food, and no reward was given during the running on the belt. The mouse ran spontaneously without any goal, so the running behavior only lasted for 4~10 seconds at once, and most of the time in a session, the mouse took a rest in between the running. On the other hand, I restricted the water consumption of rats in my experiment. Therefore, rats kept running almost without a break to get water rewards which were given at random locations on the track. When the running epoch is short, it would be possible to sequentially encode the epoch like a time cell does (MacDonald et al., 2011), but it might have been difficult to maintain such coding for a long time.

In One-cue condition, it was observed that the most of place fields of CA1 were located near the cue (**Figure 25**). When the additional cues were added on the track, the distribution of fields was uniformly spread. The difference in the distribution of field locations was clearly observed between One-cue condition and Multiple-cue condition. Rats can rely on path integration if there is no reference point, such as visual cues. In One-cue condition, the section where rats running without any cue was much longer than in Multiple-cue condition, so it would be hard the rat to keep tracking his location in One-cue condition. In addition, the input from CA3 might contribute the field formation in no cue section. The prior study where the mouse running on a linear belt with visual-tactile cues has been reported that most of the CA3 fields were not tightly bound to the

cue location but observed at a specific location in-between cue configuration (Geiller et al., 2017). Since such spatial input from CA3 was substantial only in Multiple-cue condition, it might contribute to increase the field proportion in the no cue section of Multiple-cue condition.

The current study implies different involvement of CA1 and CA3 in the association function. CA1 may be involved in all kinds of cue associations, but CA3 seems to only be involved in a situation where a lot of cue associations are required. CA1 may be able to form simple associations, but its ability is limited because of the absence of recurrent collateral. Whereas CA3 has a distinct substrate which is powerful for association (i.e., recurrent collateral), but due to the nature of the autoassociation network, it has to maintain orthogonality, so storage capacity is limited. Therefore, it seems that CA3 has been developed to be involved only in a complex situation where it is necessary and not in a simple case that CA1 is able to process. Therefore, the results of the current study could be a foundation for understanding the role of subregions of the hippocampus in memory function.

General Discussion

In this thesis, I studied how the visual scene is processed in the hippocampus, especially in the CA1 and CA3 subregions. When the rat performed the VSM task, it was confirmed that scene information was represented by rate modulation in CA1 and its output structure, the subiculum. In the VR environment, I have identified the role of the visual scene for the place field formation in CA1 and CA3. There was a difference between the two regions. The place fields of CA1 were gradually recruited as the number of cues consisting of the environment increased, whereas place fields of CA3 only emerged in response to the visual scene. These results suggested that the complex visual scene stimulus is better to recruit the hippocampal place cells rather than a simple cue and that there is a substantial difference in functions between subregions of the hippocampus.

In this thesis, I found that the scene stimulus strongly recruits hippocampal place cell. Then, it needs to be consider what the scene stimulus is. Our laboratory defines scene and object as follows (Lee et al., 2021): objects are perceptually compact things that animals perform actions on, and scenes are perceptually distributed representations that one acts in. Although the scene and object are defined exclusively, it is often difficult to distinguish these two stimulus because, in some cases, the classification of scene and object is determined based on the perception of observer. For example,

when I look at a monitor on my desk, the other objects, such as a keyboard, mouse, and pen become parts of a scene. When I focus on the pen, the pen is perceived as an object and the others are perceived as components of the scene. Like this, the same item can be perceived either object or scene depends on the observer. The previous study has reported individual difference in hippocampal dependency for an association task (Lee et al., 2014). In that task, the rat was required to choose left or right arm of T-maze based on the presented elemental cue. So, a simple tone was associated to the left side and a light was associated to right side, or vice versa. Inactivation of dorsal hippocampus impaired in about half of the rats, and the other rats showed no effect of inactivation. Therefore, this result provides evidence for that the same stimulus could be processed differently in individuals. As such although the classification of scene and object depends on the observer, we can make prediction for the probability of a stimulus being perceived as object or scene based on the shape of the stimulus. If a stimulus has clear boundary and there is a single item in the stimulus, then the probability of the stimulus being perceived as an object is quite high. On the other hand, if a stimulus contains several items so that the boundaries are overlapped or it is not likely to focus on only one item, then the stimulus is probably perceived as a scene.

Based on this definition, when considering the stimuli used in the current experiments, the scene stimuli of Chapter 1 did not

have visually compact shape with clear boundary, so they would be perceived as scenes. If an apple was presented on the monitor instead of zebra stripe pattern, it would be perceived as an object because it is a single and compact item. In One-cue, Two-cue and Three-cue conditions of Chapter 2, since the visual cues had a distance with each other, the individual cues could be easily single out from both the black background and other cues. Therefore, each cue was likely to be perceived as an object. Whereas in Multiple-cue condition, there were many visual cues arranged densely. Since their boundaries were overlapped and it seems hard to focus on a specific cue, it would be perceived as a scene.

The role of the scene in the episodic memory has been discussed in the previous studies. Tulving argued that the retrieval of episodic memory occurs through re-experiencing the past situation (Tulving, 2002), and human study has confirmed that the retrieval of episodic memory is accompanied by recalling of sensory stimulus (Rubin et al., 2003). In addition, there were claims that the scene construction is one of key processes for episodic memory retrieval (Hassabis and Maguire, 2007; Maguire and Mullally, 2013). When the episodic memory was recalled repeatedly, it either remains as episodic memory or becomes semantic memory according to the content of recalled memory (McClelland et al., 1995). Suppose that one heard the fact, for the first time, that the capital of France is Paris in his birthday party. If he reinstates ‘the capital of France is

Paris' for several times in various contexts (e.g., he heard it in class, he saw it in an internet article, etc.), then only the common memory will survive as a semantic memory. On the other hand, if he repeatedly reinstates the whole experience including the surrounding stimuli as well, then it will remain as an episodic memory that consists of various stimuli for that moment. Therefore, even after the consolidation, the scene might take part in retrieval of episodic memory, but not of semantic memory.

In Chapter 2, I observed the differences of neural representation between CA1 and CA3. CA3 cells showed distinct representations for each condition, whereas CA1 showed larger active cell ensemble and more overlapped representation. Additionally, I observed more dramatic change in coding scheme between CA1 and subiculum in Chapter 1. Even though the subiculum is a major output structure of CA1, it showed completely different activity pattern compared to CA1. The subiculum cell had broad place field and showed high activity level. In the visual scene memory task, the CA1 had focal and fine place fields that were distributed uniformly along the track. Whereas, cell population in the subiculum represented either the entire epoch before the choice (i.e., epoch from the trial start to choice) or after the choice (i.e., epoch from the choice to reward zone) (**Figure 8**), rather than representing a specific location. So, it seems that as the information flows to the downstream (i.e., from CA3 to subiculum), the coding scheme becomes dense and

overlapped. This change of coding scheme may imply the increase of generalization (Spanne and Jorntell, 2015) for efficient information processing. Subiculum cells generalized locations within an epoch so that they neglected detail information about location but emphasized which epoch the rat was located, which was cognitively more important information for performing the task. Activity of CA1 cells in the VR experiment also showed generalization for different conditions. This generalized representation of CA1 might allow the rat flexible behavior by providing signal for common features between different conditions so that the rat could take a similar action for a new condition. Therefore, it seems that the neural representation evolves in the flow of information for flexible and goal-oriented behavior.

In my experiment, it was confirmed that the involvement of the hippocampus was large when dealing with scene stimuli that require a lot of association. Although only visual stimulus was tested here, this result might be extended to other modalities. It is known that olfactory and auditory information come through entorhinal cortex to the hippocampus (Burwell, 2000; Kerr et al., 2007; Agster and Burwell, 2013), and there are physiological evidence that the hippocampal neurons represent odor or tone frequency (MacDonald et al., 2013; Igarashi et al., 2014; Aronov et al., 2017). In particular, in the Aronov, when the rat pressed the joystick, a tone of 2 kHz was produced, and the frequency gradually went up, so the rat was

required to release the joystick when a certain frequency range was reached. In this experiment, although the task was performed only in a fixed place, in front of the joystick, the place cell firing was modulated by the frequency even when the spatial component was eliminated. In addition, it has been reported that there are cells in the hippocampus responding to various visual images related to a single concept (Quiroga et al., 2005). Considering these empirical results comprehensively, it seems possible that the hippocampus is playing a role of a relational network that forms an association between sensory stimulus and concepts (Alvarez and Squire, 1994; Levy, 1996; Eichenbaum et al., 1999).

Bibliography

Addis DR, Wong AT, Schacter DL (2007) Remembering the past and imagining the future: Common and distinct neural substrates during event construction and elaboration. Neuropsychologia 45:1363-1377.

Aggleton JP, Christiansen K (2015) The subiculum: the heart of the extended hippocampal system. Prog Brain Res 219:65-82.

Agster KL, Burwell RD (2013) Hippocampal and subicular efferents and afferents of the perirhinal, postrhinal, and entorhinal cortices of the rat. Behav Brain Res 254:50-64.

Ahn JR, Lee I (2015) Neural correlates of object-associated choice behavior in the perirhinal cortex of rats. J Neurosci 35:1692-1705.

Ahn JR, Lee HW, Lee I (2019) Rhythmic Pruning of Perceptual Noise for Object Representation in the Hippocampus and Perirhinal Cortex in Rats. Cell Rep 26:2362-2376 e2364.

Alme CB, Miao CL, Jezek K, Treves A, Moser EI, Moser MB (2014) Place cells in the hippocampus: Eleven maps for eleven rooms. P Natl Acad Sci USA 111:18428-18435.

Alvarez P, Squire LR (1994) Memory Consolidation and the Medial Temporal-Lobe - a Simple Network Model. P Natl Acad Sci USA 91:7041-7045.

Amaral DG, Ishizuka N, Claiborne B (1990) Neurons, Numbers and

the Hippocampal Network. Progress in Brain Research 83:1-11.

Amaral DG, Dolorfo C, Alvarez-Royo P (1991) Organization of CA1 projections to the subiculum: a PHA-L analysis in the rat. Hippocampus 1:415-435.

Andelman F, Hoofien D, Goldberg I, Aizenstein O, Neufeld MY (2010) Bilateral hippocampal lesion and a selective impairment of the ability for mental time travel. Neurocase 16:426-435.

Andersen P, Bliss TVP, Lomo T, Olsen LI, Skrede KK (1969) Lamellar Organization of Hippocampal Excitatory Pathways. Acta Physiol Scand 76:A4-&.

Aronov D, Nevers R, Tank DW (2017) Mapping of a non-spatial dimension by the hippocampal-entorhinal circuit. Nature 543:719-722.

Bains JS, Longacher JM, Staley KJ (1999) Reciprocal interactions between CA3 network activity and strength of recurrent collateral synapses. Nature Neuroscience 2:720-726.

Barnes CA, McNaughton BL, Mizumori SJ, Leonard BW, Lin LH (1990) Comparison of spatial and temporal characteristics of neuronal activity in sequential stages of hippocampal processing. Prog Brain Res 83:287-300.

Bos JJ, Vinck M, van Mourik-Donga LA, Jackson JC, Witter MP, Pennartz CMA (2017) Perirhinal firing patterns are sustained across large spatial segments of the task environment. Nat

Commun 8:15602.

Bourboulou R, Marti G, Michon FX, El Feghaly E, Nouguier M, Robbe D, Koenig J, Epsztein J (2019) Dynamic control of hippocampal spatial coding resolution by local visual cues. Elife 8.

Brun VH, Otnass MK, Molden S, Steffenach HA, Witter MP, Moser MB, Moser EI (2002) Place cells and place recognition maintained by direct entorhinal-hippocampal circuitry. Science 296:2243-2246.

Burwell RD (2000) The parahippocampal region: corticocortical connectivity. Ann N Y Acad Sci 911:25-42.

Burwell RD, Amaral DG (1998) Cortical afferents of the perirhinal, postrhinal, and entorhinal cortices of the rat. J Comp Neurol 398:179-205.

Catanese J, Viggiano A, Cerasti E, Zugaro MB, Wiener SI (2014) Retrospectively and prospectively modulated hippocampal place responses are differentially distributed along a common path in a continuous T-maze. J Neurosci 34:13163-13169.

Cembrowski MS, Phillips MG, DiLisio SF, Shields BC, Winnubst J, Chandrashekar J, Bas E, Spruston N (2018) Dissociable Structural and Functional Hippocampal Outputs via Distinct Subiculum Cell Classes. Cell.

Cenquizca LA, Swanson LW (2007) Spatial organization of direct hippocampal field CA1 axonal projections to the rest of the

cerebral cortex. Brain research reviews 56:1-26.

Claiborne BJ, Amaral DG, Cowan WM (1986) A Light and Electron-Microscopic Analysis of the Mossy Fibers of the Rat Dentate Gyrus. Journal of Comparative Neurology 246:435-458.

Colgin LL, Moser EI, Moser MB (2008) Understanding memory through hippocampal remapping. Trends Neurosci 31:469-477.

Debanne D, Gahwiler BH, Thompson SM (1998) Long-term synaptic plasticity between pairs of individual CA3 pyramidal cells in rat hippocampal slice cultures. J Physiol-London 507:237-247.

Delcasso S, Huh N, Byeon JS, Lee J, Jung MW, Lee I (2014) Functional relationships between the hippocampus and dorsomedial striatum in learning a visual scene-based memory task in rats. J Neurosci 34:15534-15547.

Deshmukh SS, Knierim JJ (2011) Representation of non-spatial and spatial information in the lateral entorhinal cortex. Front Behav Neurosci 5:69.

Eichenbaum H (2000) A cortical-hippocampal system for declarative memory. Nat Rev Neurosci 1:41-50.

Eichenbaum H, Dudchenko P, Wood E, Shapiro M, Tanila H (1999) The hippocampus, memory, and place cells: is it spatial memory or a memory space? Neuron 23:209-226.

Ferbinteanu J, Shapiro ML (2003) Prospective and retrospective memory coding in the hippocampus. Neuron 40:1227-1239.

Fyhn M, Hafting T, Treves A, Moser MB, Moser EI (2007)

Hippocampal remapping and grid realignment in entorhinal cortex. Nature 446:190-194.

Geiller T, Fattahi M, Choi JS, Royer S (2017) Place cells are more strongly tied to landmarks in deep than in superficial CA1. Nat Commun 8:14531.

Geva-Sagiv M, Romani S, Las L, Ulanovsky N (2016) Hippocampal global remapping for different sensory modalities in flying bats. Nat Neurosci 19:952-958.

Gothard KM, Skaggs WE, McNaughton BL (1996) Dynamics of mismatch correction in the hippocampal ensemble code for space: interaction between path integration and environmental cues. J Neurosci 16:8027-8040.

Guzowski JF, Knierim JJ, Moser EI (2004) Ensemble dynamics of hippocampal regions CA3 and CA1. Neuron 44:581-584.

Hafting T, Fyhn M, Molden S, Moser MB, Moser EI (2005) Microstructure of a spatial map in the entorhinal cortex. Nature 436:801-806.

Hallock HL, Griffin AL (2013) Dynamic coding of dorsal hippocampal neurons between tasks that differ in structure and memory demand. Hippocampus 23:169-186.

Hampson RE, Deadwyler SA (2003) Temporal firing characteristics and the strategic role of subicular neurons in short-term memory. Hippocampus 13:529-541.

Hargreaves EL, Rao G, Lee I, Knierim JJ (2005) Major dissociation

between medial and lateral entorhinal input to dorsal hippocampus. Science 308:1792-1794.

Hassabis D, Maguire EA (2007) Deconstructing episodic memory with construction. Trends Cogn Sci 11:299-306.

Hassabis D, Kumaran D, Maguire EA (2007a) Using imagination to understand the neural basis of episodic memory. J Neurosci 27:14365-14374.

Hassabis D, Kumaran D, Vann SD, Maguire EA (2007b) Patients with hippocampal amnesia cannot imagine new experiences. Proc Natl Acad Sci U S A 104:1726-1731.

Hebb DO (1964) The organization of behavior: A neuropsychological theory. New York: John Wiley.

Henriksen EJ, Colgin LL, Barnes CA, Witter MP, Moser MB, Moser EI (2010) Spatial representation along the proximodistal axis of CA1. Neuron 68:127-137.

Hetherington PA, Shapiro ML (1997) Hippocampal place fields are altered by the removal of single visual cues in a distance-dependent manner. Behav Neurosci 111:20-34.

Hoydal OA, Skytoen ER, Andersson SO, Moser MB, Moser EI (2019) Object-vector coding in the medial entorhinal cortex. Nature 568:400-404.

Igarashi KM, Lu L, Colgin LL, Moser MB, Moser EI (2014) Coordination of entorhinal-hippocampal ensemble activity during associative learning. Nature 510:143-147.

Ishizuka N, Weber J, Amaral DG (1990) Organization of Intrahippocampal Projections Originating from Ca3 Pyramidal Cells in the Rat. Journal of Comparative Neurology 295:580-623.

Jung MW, Wiener SI, McNaughton BL (1994) Comparison of spatial firing characteristics of units in dorsal and ventral hippocampus of the rat. J Neurosci 14:7347-7356.

Kerr KM, Agster KL, Furtak SC, Burwell RD (2007) Functional neuroanatomy of the parahippocampal region: the lateral and medial entorhinal areas. Hippocampus 17:697-708.

Kim JJ, Fanselow MS (1992) Modality-specific retrograde amnesia of fear. Science 256:675-677.

Kim S, Lee J, Lee I (2012a) The hippocampus is required for visually cued contextual response selection, but not for visual discrimination of contexts. Front Behav Neurosci 6:66.

Kim SM, Ganguli S, Frank LM (2012b) Spatial information outflow from the hippocampal circuit: distributed spatial coding and phase precession in the subiculum. J Neurosci 32:11539-11558.

Kishi T, Tsumori T, Ono K, Yokota S, Ishino H, Yasui Y (2000) Topographical organization of projections from the subiculum to the hypothalamus in the rat. J Comp Neurol 419:205-222.

Kitamura T, Ogawa SK, Roy DS, Okuyama T, Morrissey MD, Smith LM, Redondo RL, Tonegawa S (2017) Engrams and circuits crucial for systems consolidation of a memory. Science

356:73-78.

Knight R (1996) Contribution of human hippocampal region to novelty detection. Nature 383:256-259.

Lacy JW, Yassa MA, Stark SM, Muftuler LT, Stark CEL (2011) Distinct pattern separation related transfer functions in human CA3/dentate and CA1 revealed using high-resolution fMRI and variable mnemonic similarity. Learn Memory 18:15-18.

Laurberg S (1979) Commissural and Intrinsic Connections of the Rat Hippocampus. Journal of Comparative Neurology 184:685-708.

Le Duigou C, Simonnet J, Telenczuk MT, Fricker D, Miles R (2014) Recurrent synapses and circuits in the CA3 region of the hippocampus: an associative network. Front Cell Neurosci 7.

Lee I, Kim J (2010) The shift from a response strategy to object-in-place strategy during learning is accompanied by a matching shift in neural firing correlates in the hippocampus. Learn Mem 17:381-393.

Lee I, Yoganarasimha D, Rao G, Knierim JJ (2004) Comparison of population coherence of place cells in hippocampal subfields CA1 and CA3. Nature 430:456-459.

Lee KJ, Park SB, Lee I (2014) Elemental or contextual? It depends: individual difference in the hippocampal dependence of associative learning for a simple sensory stimulus. Front Behav Neurosci 8:217.

Lee SM, Jin SW, Park SB, Park EH, Lee CH, Lee HW, Lim HY, Yoo

SW, Ahn JR, Shin J, Lee SA, Lee I (2021) Goal-directed interaction of stimulus and task demand in the parahippocampal region. Hippocampus.

Leutgeb JK, Leutgeb S, Moser MB, Moser EI (2007) Pattern separation in the dentate gyrus and CA3 of the hippocampus. Science 315:961-966.

Leutgeb S, Leutgeb JK, Treves A, Moser MB, Moser EI (2004) Distinct ensemble codes in hippocampal areas CA3 and CA1. Science 305:1295-1298.

Leutgeb S, Leutgeb JK, Barnes CA, Moser EI, McNaughton BL, Moser MB (2005) Independent codes for spatial and episodic memory in hippocampal neuronal ensembles. Science 309:619-623.

Lever C, Burton S, Jeewajee A, O'Keefe J, Burgess N (2009) Boundary vector cells in the subiculum of the hippocampal formation. J Neurosci 29:9771-9777.

Levy WB (1996) A sequence predicting CA3 is a flexible associator that learns and uses context to solve hippocampal-like tasks. Hippocampus 6:579-590.

MacDonald CJ, Lepage KQ, Eden UT, Eichenbaum H (2011) Hippocampal "time cells" bridge the gap in memory for discontiguous events. Neuron 71:737-749.

MacDonald CJ, Carrow S, Place R, Eichenbaum H (2013) Distinct hippocampal time cell sequences represent odor memories in

immobilized rats. J Neurosci 33:14607-14616.

Maguire EA, Mullally SL (2013) The hippocampus: a manifesto for change. J Exp Psychol Gen 142:1180-1189.

Markus EJ, Qin YL, Leonard B, Skaggs WE, McNaughton BL, Barnes CA (1995) Interactions between location and task affect the spatial and directional firing of hippocampal neurons. J Neurosci 15:7079-7094.

McClelland JL, McNaughton BL, O'Reilly RC (1995) Why there are complementary learning systems in the hippocampus and neocortex: insights from the successes and failures of connectionist models of learning and memory. Psychol Rev 102:419-457.

Mcnaughton BL, Morris RGM (1987) Hippocampal Synaptic Enhancement and Information-Storage within a Distributed Memory System. Trends in Neurosciences 10:408-415.

McNaughton BL, Barnes CA, O'Keefe J (1983) The contributions of position, direction, and velocity to single unit activity in the hippocampus of freely-moving rats. Exp Brain Res 52:41-49.

Mizuseki K, Royer S, Diba K, Buzsaki G (2012) Activity dynamics and behavioral correlates of CA3 and CA1 hippocampal pyramidal neurons. Hippocampus 22:1659-1680.

Moser EI, Kropff E, Moser MB (2008) Place cells, grid cells, and the brain's spatial representation system. Annu Rev Neurosci 31:69-89.

Mullally SL, Intraub H, Maguire EA (2012) Attenuated Boundary Extension Produces a Paradoxical Memory Advantage in Amnesic Patients. Curr Biol 22:261-268.

Muller RU, Kubie JL (1987) The effects of changes in the environment on the spatial firing of hippocampal complex-spike cells. J Neurosci 7:1951-1968.

Muller RU, Kubie JL (1989) The firing of hippocampal place cells predicts the future position of freely moving rats. J Neurosci 9:4101-4110.

O'Keefe J, Dostrovsky J (1971) The hippocampus as a spatial map. Preliminary evidence from unit activity in the freely-moving rat. Brain Res 34:171-175.

O'Keefe J, Nadel L (1978) The Hippocampus as a Cognitive Map. In. Britain: Oxford Univ. Press.

O'Mara SM, Sanchez-Vives MV, Brotons-Mas JR, O'Hare E (2009) Roles for the subiculum in spatial information processing, memory, motivation and the temporal control of behaviour. Prog Neuropsychopharmacol Biol Psychiatry 33:782-790.

Olson JM, Tongprasearth K, Nitz DA (2017) Subiculum neurons map the current axis of travel. Nat Neurosci 20:170-172.

Packard MG, McGaugh JL (1996) Inactivation of hippocampus or caudate nucleus with lidocaine differentially affects expression of place and response learning. Neurobiol Learn Mem 65:65-72.

Paxinos G, Watson C (2009) The Rat Brain in Stereotaxic Coordianates, 6th Edition. London, UK: Elsevier.

Quirk GJ, Muller RU, Kubie JL (1990) The firing of hippocampal place cells in the dark depends on the rat's recent experience. J Neurosci 10:2008-2017.

Quiroga RQ, Reddy L, Kreiman G, Koch C, Fried I (2005) Invariant visual representation by single neurons in the human brain. Nature 435:1102-1107.

Race E, Keane MM, Verfaellie M (2011) Medial Temporal Lobe Damage Causes Deficits in Episodic Memory and Episodic Future Thinking Not Attributable to Deficits in Narrative Construction. Journal of Neuroscience 31:10262-10269.

Rolls ET (2007) An attractor network in the hippocampus: Theory and neurophysiology. Learn Memory 14:714-731.

Rubin DC, Schrauf RW, Greenberg DL (2003) Belief and recollection of autobiographical memories. Mem Cognit 31:887-901.

Sargolini F, Fyhn M, Hafting T, McNaughton BL, Witter MP, Moser MB, Moser EI (2006) Conjunctive representation of position, direction, and velocity in entorhinal cortex. Science 312:758-762.

Scoville WB, Milner B (1957) Loss of recent memory after bilateral hippocampal lesions. J Neurol Neurosurg Psychiatry 20:11-21.

Sharp PE (1997) Subicular cells generate similar spatial firing patterns in two geometrically and visually distinctive

environments: comparison with hippocampal place cells. Behav Brain Res 85:71-92.

Sharp PE (1999) Subicular place cells expand or contract their spatial firing pattern to fit the size of the environment in an open field but not in the presence of barriers: comparison with hippocampal place cells. Behav Neurosci 113:643-662.

Sharp PE, Green C (1994) Spatial correlates of firing patterns of single cells in the subiculum of the freely moving rat. J Neurosci 14:2339-2356.

Skaggs WE, McNaughton BL (1992) Computational approaches to hippocampal function. Current Opinion in Neurobiology 2:209-211.

Skaggs WE, McNaughton BL (1993) An information-theoretic approach to deciphering the hippocampal code.

Skaggs WE, McNaughton BL (1998) Spatial firing properties of hippocampal CA1 populations in an environment containing two visually identical regions. J Neurosci 18:8455-8466.

Skaggs WE, McNaughton BL, Wilson MA, Barnes CA (1996) Theta phase precession in hippocampal neuronal populations and the compression of temporal sequences. Hippocampus 6:149-172.

Solstad T, Boccara CN, Kropff E, Moser MB, Moser EI (2008) Representation of geometric borders in the entorhinal cortex. Science 322:1865-1868.

Spanne A, Jorntell H (2015) Questioning the role of sparse coding in

the brain. Trends Neurosci 38:417-427.

Squire LR, Wixted JT (2011) The cognitive neuroscience of human memory since H.M. Annu Rev Neurosci 34:259-288.

Steward O (1976) Topographic organization of the projections from the entorhinal area to the hippocampal formation of the rat. J Comp Neurol 167:285-314.

Swanson LW, Wyss JM, Cowan WM (1978) An autoradiographic study of the organization of intrahippocampal association pathways in the rat. J Comp Neurol 181:681-715.

Tanila H (1999) Hippocampal place cells can develop distinct representations of two visually identical environments. Hippocampus 9:235-246.

Tolman EC (1948) Cognitive Maps in Rats and Men. Psychol Rev 55:189-208.

Treves A, Rolls ET (1992) Computational constraints suggest the need for two distinct input systems to the hippocampal CA3 network. Hippocampus 2:189-199.

Tsao A, Moser MB, Moser EI (2013) Traces of experience in the lateral entorhinal cortex. Curr Biol 23:399-405.

Tulving E (2002) Episodic memory: from mind to brain. Annu Rev Psychol 53:1-25.

Vazdarjanova A, Guzowski JF (2004) Differences in hippocampal neuronal population responses to modifications of an environmental context: evidence for distinct, yet

complementary, functions of CA3 and CA1 ensembles. J Neurosci 24:6489-6496.

Villette V, Malvache A, Tressard T, Dupuy N, Cossart R (2015) Internally Recurring Hippocampal Sequences as a Population Template of Spatiotemporal Information. Neuron 88:357-366.

Vinogradova OS (2001) Hippocampus as comparator: role of the two input and two output systems of the hippocampus in selection and registration of information. Hippocampus 11:578-598.

Wang C, Chen X, Lee H, Deshmukh SS, Yoganarasimha D, Savelli F, Knierim JJ (2018) Egocentric coding of external items in the lateral entorhinal cortex. Science 362:945-949.

Witter MP (2006) Connections of the subiculum of the rat: topography in relation to columnar and laminar organization. Behav Brain Res 174:251-264.

Witter MP, Groenewegen HJ, Lopes da Silva FH, Lohman AH (1989) Functional organization of the extrinsic and intrinsic circuitry of the parahippocampal region. Prog Neurobiol 33:161-253.

Witter MP, Wouterlood FG, Naber PA, Van Haeften T (2000) Anatomical organization of the parahippocampal-hippocampal network. Ann N Y Acad Sci 911:1-24.

Witter MP, Canto CB, Couey JJ, Koganezawa N, O'Reilly KC (2014) Architecture of spatial circuits in the hippocampal region. Philos Trans R Soc Lond B Biol Sci 369:20120515.

Wood ER, Dudchenko PA, Robitsek RJ, Eichenbaum H (2000)

Hippocampal neurons encode information about different types of memory episodes occurring in the same location. Neuron 27:623-633.

Zola-Morgan S, Squire LR, Amaral DG (1986) Human amnesia and the medial temporal region: enduring memory impairment following a bilateral lesion limited to field CA1 of the hippocampus. J Neurosci 6:2950-2967.

국문초록

해마 하위 영역 CA1과 CA3의 장면 자극에 기반한 장소 표상 형성 연구

이현우

우리는 과거의 경험을 떠올릴 때 그 때를 묘사하는 문장을 떠올리는 것이 아니라 경험 한 순간에 보았던 것, 들렸던 소리, 느꼈던 감정 등이 복합적으로 어우러진 장면을 떠올리게 된다. 이렇게 장면은 일화 기억을 구성하는 중요한 요소라 할 수 있기에 장면 자극이 뇌에서 어떻게 표상되며 저장되는지를 연구하는 것은 우리 기억의 형성과 저장, 재인 과정을 이해하는데 있어 매우 중요하다고 볼 수 있다. 뇌에서 일화 기억을 담당한다고 알려진 영역은 해마로써, 해마에 손상을 입은 환자들 또는 동물들이 과거의 기억을 인출하거나 새로운 기억을 형성하는데 있어 어려움을 겪는다는 것이 여러 실험을 통해 보고 된 바 있다. 해마는 일화 기억뿐만 아니라 공간에 대한 지도를 형성하는 데에도 관여하는데, 특히, 설치류 해마에서 관찰 되는 장소 세포가 이러한 해마의 기능들을 수행하는데 핵심적인 역할을 하는 것으로 알려져 있

다. 하지만 장소 세포는 주로 쥐가 공간을 탐색하는 과정에서의 발화 패턴을 관측한 연구가 주를 이루었으며 장면 자극이 개별 장소 세포의 발화 패턴을 통해 어떻게 표상이 되는지에 대한 연구는 미미한 수준이다.

이 논문에서 나는 장면 자극이 해마의 장소 세포에서 어떻게 표상되는지를 알아보고자 쥐가 모니터에 제시 된 장면 자극을 보고 오른쪽이나 왼쪽을 선택해야 하는 과제를 수행 할 때 해마의 하위 영역인 CA1 과 해마의 정보를 전달받아 뇌의 다른 영역으로 정보를 전달하는 해마이행부의 단일 세포 활동을 측정하였다. 그 결과 CA1 과 해마이행부에서 관찰 된 장소 세포들이 장면 자극에 따른 발화율 변화를 보인다는 것을 확인 할 수 있었다. 이에 더하여 나는 해마의 장소 세포들이 장소장을 형성하기 위해서 필요한 시각 자극이 무엇이며, 이에 장면 자극이 어떤 역할을 하는지 확인하기 위해 가상 환경을 이용한 실험을 수행하였다. 이 실험에서는 쥐가 선형 트랙을 달릴 때, 빈 공간에서 시작하여 장면 자극을 형성 할 때까지 시각 자극을 하나씩 추가하면서 해마의 하위 영역인 CA1 과 CA3 의 장소 세포 활동을 측정 하는 과정을 통해 어떤 시각 자극이 장소 세포의 장소장 형성에 가장 큰 영향을 미치는 것인지 알아보았다. 그 결과 CA1 의 장소 세포는 간단한

시각 자극의 추가에도 장소장을 잘 형성하는 모습을 보인 반면 CA3 의 장소 세포들은 충분한 시각 자극이 모여서 장면 자극을 형성 한 경우에 장소장을 형성하는 것이 관찰되었다. 이러한 일련의 실험을 통하여 나는 장면 자극이 해마의 장소 세포 발화를 통해 표상되며, 해마의 하위 영역이 모두 장면 자극 처리에 관여하지만 그 중에서도 특히 CA3 가 장면 자극을 처리 할 때에 한하여 큰 활성을 보인다는 것을 밝혔다.